Exploration of Bis-amino Acid Scaffolds Designed to Self Assemble

by

Megan K. Macala

B.S. John Carroll University, 2004

Submitted to the Graduate Faculty of

Arts and Science in partial fulfillment

of the requirements for the degree of

Master in Science

University of Pittsburgh

2007

UNIVERSITY OF PITTSBURGH

FACULTY OF ARTS AND SCIENCES

This thesis was presented

by

Megan K. Macala

It was defended on

February 26th, 2007

and approved by

Toby M. Chapman, Associate Professor, Department of Chemistry

Craig S. Wilcox, Professor, Department of Chemistry

Thesis Director: Chris E. Schafmiester, Assistant Professor, Department of Chemistry

Exploration of Bis-amino Acid Scaffolds Designed to Self Assemble

Megan K. Macala, M.S.

University of Pittsburgh, 2007

Based on theoretical models scaffold **13** was predicted to self assemble through intermolecular hydrogen bonds. The synthesis of scaffold **13** (napthylalanine-Pro4(2*S*4*R*)-Pro4(*2R*4*S*)-Pro4(2*S*4*R*)-Pro4(2*R*4*S*)) was successfully synthesized using standard Fmoc Solid Phase Peptide Synthesis. Connectivity was confirmed through full structural characterization (^{1}H NMR, COSY, HMQC, HMBC, ROESY). Scaffold **13** was probed for its ability to self-assemble in $DMSO_{d6}$ in the presence of 0.2 % TFA (13 mM – 4 mM). Our hypothesis for self-assembly of scaffold **13** was not supported under any of the conditions explored. ROESY correlations failed to indicate self-assembly between interacting scaffolds and a variable temperature (25 to 80 °C) NMR study at three separate concentrations (13 mM, 4mM, 1 mM) also failed to provide evidence of self-assembly.

TABLE OF CONTENTS

LIST OF TABLES

LIST OF FIGURES

LIST OF SCHEMES

LIST OF ABBREVIATIONS

BOC	tert-butoxycarbonyl
DCM	dichloromethane
DIPEA	diisopropylethylamine
DKP	diketopiperazine
DMF	dimethylformamide
DMSO	dimethylsulfoxide
DVB	divinylbenzene
FMOC	9-fluorenylmethoxycarbonyl
HATU	O-(7-Azabenzotriazol-1-yl)-*N*,*N*,*N*',*N*'-tetramethyluroniumhexafluorophosphate
MSNT	1-(Mesitylene-2-sulfonyl)-3-nitro-1H-1,2,4-triazole
NMP	1-methyl-2-pyrrolidinone
TFA	trifluoroacetic acid
TfOH	triflic acid

1.0 NATURE AS INSPIRATION

The natural world has long provided inspiration for scientists and scholars. With a subset of molecules, nature routinely constructs large, intricate, functional structures, used in virtually every significant biological process. Nature effortlessly builds an enormous and diverse array of highly efficient nanoscale machines. Biological molecular machines can be as simple as the heme containing proteins myoglobin and hemoglobin which shuttle molecular oxygen and carbon dioxide to and from living cells or more complex such as highly specific proteases, nucleases, and kinases designed to enable the efficient chemical modification of numerous biomolecules[1]. Even more complicated molecular machines can be identified, such as the ribosome, responsible for translation of messenger RNA into proteins and microtubles, which play a crucial role in cell division[1]. The level of sophistication with which nature assembles these nano-scale devices provides an enormous source of inspiration. She challenges us to mimic her ability to control structure at the molecular level in a quest to produce ever more intricate materials and devices.

Many biological processes are governed by selective interactions between discrete molecules. Once a protein is assembled through biosynthesis, it naturally folds under physiological conditions into its functional form in a process known as protein folding[2]. It is believed that unfolded proteins do not simply fold by sampling all possible conformations randomly until the lowest free energy is encountered. This is not feasible based on a practical

time scale since peptide chains can adopt a vast number of conformations. It is believed that protein folding is largely ordered although it is not necessarily a direct pathway. Some proteins fold through the assistance of accessory proteins, such as molecular chaperones which can prevent improper folding and aggregation of proteins. Hydrophobic forces largely drive protein folding in which hydrophobic side chains are often hidden from the aqueous environment while the hydrophilic groups are exposed[3]. Although much progress has been made in understanding the underlying mechanism of protein folding, we still do not fully understand how or why proteins adopt their active tertiary conformations. Chemists have made considerable efforts in designing non-natural peptides that emulate the highly evolved characteristics of proteins.

1.1 NANOTECHNOLOGY

Nanotechnology is concerned with the precise control over the placement of atoms in three dimensional space, especially with respect to the production of useful nanoscale devices. Although the field remains in its infancy, nanotechnology ultimately brings with it the promise of radical new technologies through precise, rational control over structure.

Two major strategies have been employed for the construction of nanoscale structures. The first is a top-down approach in which the final structure is produced by stripping excess material. A common top-down approach involves photolithographic patterning techniques using optical sources. A key advantage of the top-down approach is that no assembly step is needed. Optical lithography is a relatively mature field with techniques capable of reaching dimensions just below 100 nanometers[4]. However, the disadvantages to this approach include physical and

economic costs that limit the use of this technology in the construction of smaller, more intricate structures. To the contrary, the bottom-up approach assembles nanostructures molecule by molecule, even atom by atom[4]. The bottom up approach requires a set of building blocks that can be assembled to create larger, more complex structures. The shape of the parent structure is dependent on the nature and sequence of the building blocks. Nature uses this approach in the construction of peptides and nucleic acids. Polymer chemistry utilizes this approach in the construction of polymeric materials with unique bulk properties. The ultimate limitations of this approach are the building blocks themselves. Although both approaches are useful, the bottom up approach is likely to become an important component of nano-material manufacture since it provides the greatest control of placement of atoms and molecules[4]. With the bottom-up approach as a viable option to precisely control molecular architecture, chemists are able to synthesize molecules and assemble them in such a way as to produce useful nanoscale devices.

1.2 UNNATURAL MONOMERS

Numerous unnatural monomers have been designed which can be assembled into larger oligomeric structures. Oligomers constructed from these monomers that fold into a well defined secondary structures, foldamers, are governed by weak, usually intramolecular noncovalent interactions that stabilize the resulting secondary and tertiary structures of these compounds in solution[5]. Typically oligomers are assembled through single bonds between monomers such as β-amino acids[6, 7], sulfonamidopeptides[8], oliopyrrolinones[9], oligoanthranilamides[10], oligoureas[11-15], phenylacetylene oligomers[16, 17], and vinylogous amino acids[18].

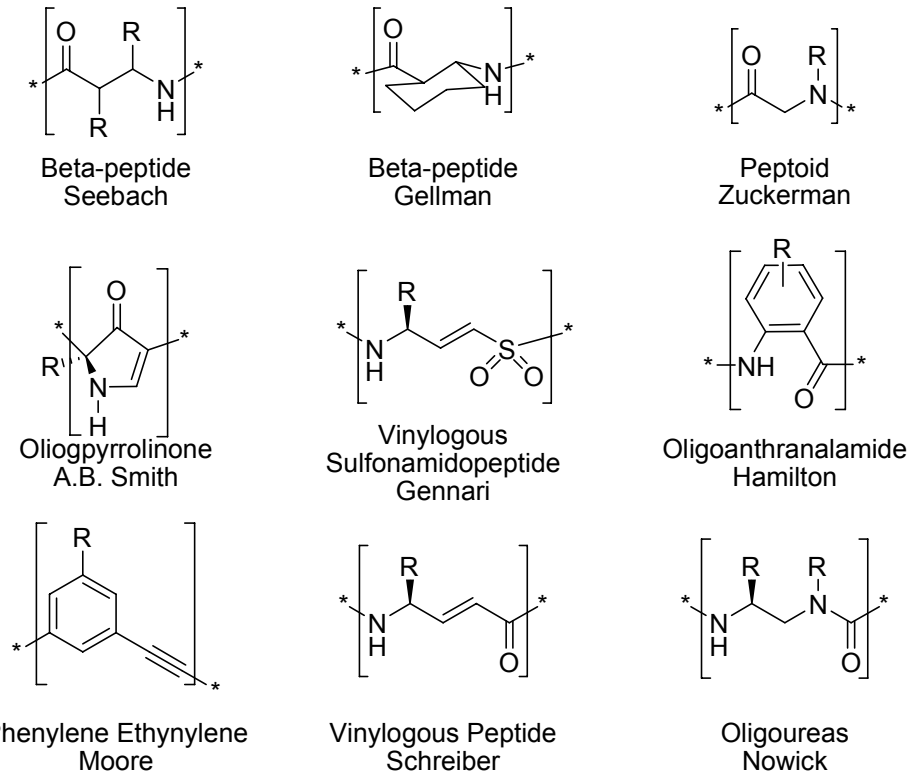

Figure 1. Unnatural Amino Acids

One successful example in the research of synthetic foldamers has been the development of U-turns to control the secondary structure in triureas that serve as functional mimics of their biological counterparts, the β-turn. Intramolecularly hydrogen bonded ten-membered ring

conformations in dilute chloroform solutions have been shown to control the structure of an oligourea backbone (Figure 2)[15]. This work has been extended to a variety of acylic diureas in which hydrogen bonding creates conformationally well-defined structures [11, 12, 14, 19, 20], however, the majority of examples which have demonstrated secondary structure have been in aprotic organic solvents.

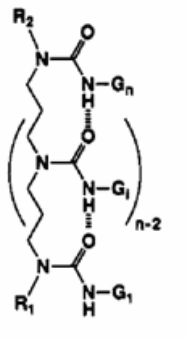

Figure 2. Intramolecular hydrogen bonded rings formed in triureas.

Another example involving the use of intramolecular hydrogen bonding to control conformation utilizes anthranilamide oligomers[10]. Intramolecular hydrogen bonding in addition to the trans requirement of the amide bond is responsible for the preferred conformation (Figure 3). The x-ray structure exhibits a helical arrangement of the rings stabilized by intramolecular hydrogen bonds ($NH_a\cdots N$, 2.20 and 2.21 Å); $NH_a\cdots OC$, 1.82 and 2.02 Å). The terminal anthranilamide rings are 5.41 Å apart. Supporting evidence of the intramolecularly hydrogen bonded network was provided by a variable temperature NMR experiment (from -40 to 40 °C) in which shifting of the amide-NH resonances in a 10 mM solution of the compound in 20% $DMSO_{d6}$/80% $CDCl_3$ was assessed. The intramolecular hydrogen bonded amide protons exhibited a small variation with temperature (2.9×10^{-3} and 1.1×10^{-3} ppm) in the polar solvent system.

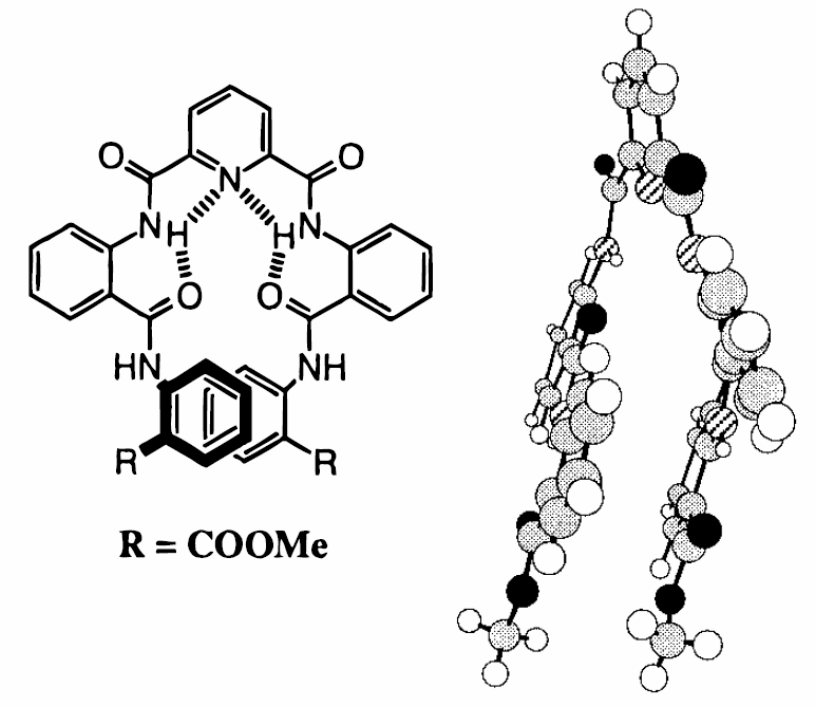

Figure 3. Intramolecular hydrogen bonded anthranilamide oligomer (left). X-ray structure (right).

The control of specific functionality in space leads to numerous potential applications. Among these is the possibility for the generation of species capable of binding to small molecules[21]. Dibenzodiazocines are rigid species that are able to orient their functional groups, such as carboxylic acids, at an angle of approximately 120° with respect to one another, allowing these molecules to serve as synthetic receptors[22]. These functional groups are well-arranged for binding several same guests such as 9-ethyladenine and biotin methyl ester through multiple hydrogen bonds.

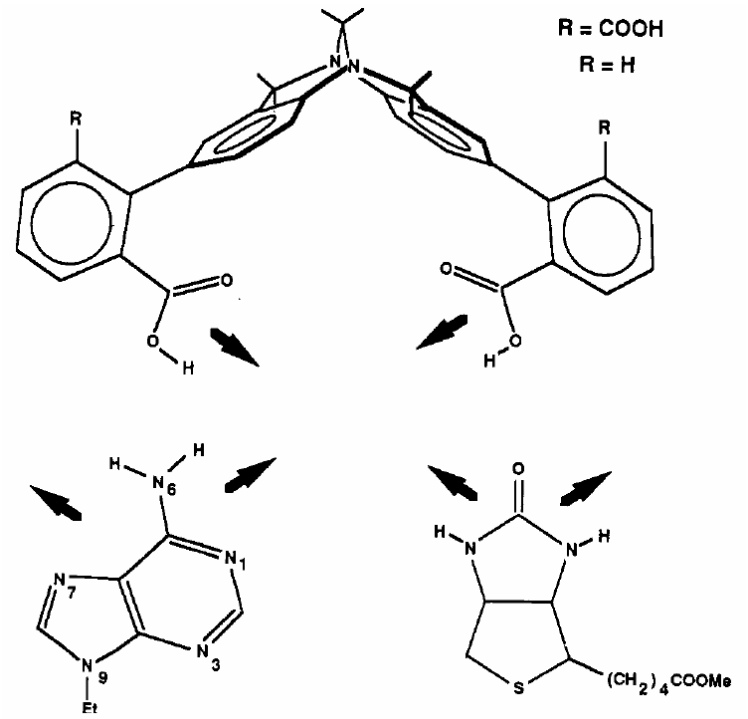

Figure 4. Orderly functional group dyads as synthetic hosts

Dibenzodiazocines position the carboxylic acids in the required configuration as a direct consequence of the rigid nature of their backbone. The barrier for the aryl-aryl bond rotation for host (R=COOH) was determined to be 15.0 kcal/mol in THF-$_{d8}$ or methanol-$_{d4}$. The dibenzodiazocines host (R=COOH) binds to 9-ethyladenine in THF-$_{d8}$ quite strongly demonstrating K*a* of 140 M^{-1} [22].

Others have achieved well-defined structures through the utilization of pi-stacking between subunits, rigidification to minimize conformational degrees of freedom, donor-acceptor interactions, and destabilization of unwanted conformations[10]. Although significant progress has been achieved in this area, there remain numerous problems with some of the previously described building blocks: solubility problems, long coupling times, uncertainty with regard to the oligomeric folding unique to the building blocks, and high degree of symmetry.

1.3 BIS-AMINO ACIDS

Our research group has designed an approach for the synthesis of molecular scaffolds that possess well-defined structures in aqueous solution. The scaffolds are assembled from monomers through solid phase peptide synthesis. Following synthesis, the scaffolds are rigidified through the formation of a pair of bonds between the cyclic monomers. Elimination of multiple degrees of freedom from within each scaffold ensures that the synthetic structures are incapable of folding, thus eliminating difficulties associated with the prediction of the folded structures in solution. These compounds adopt fixed and predictable conformations that are readily modeled computationally. By varying the monomers used to construct each scaffold, a diverse array of molecular architectures can be obtained (Figure 5)

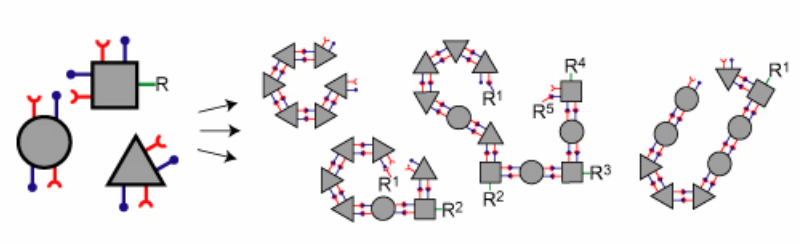

Figure 5. Cartoon of monomers that can be incorporated into an array of structurally defined scaffolds.

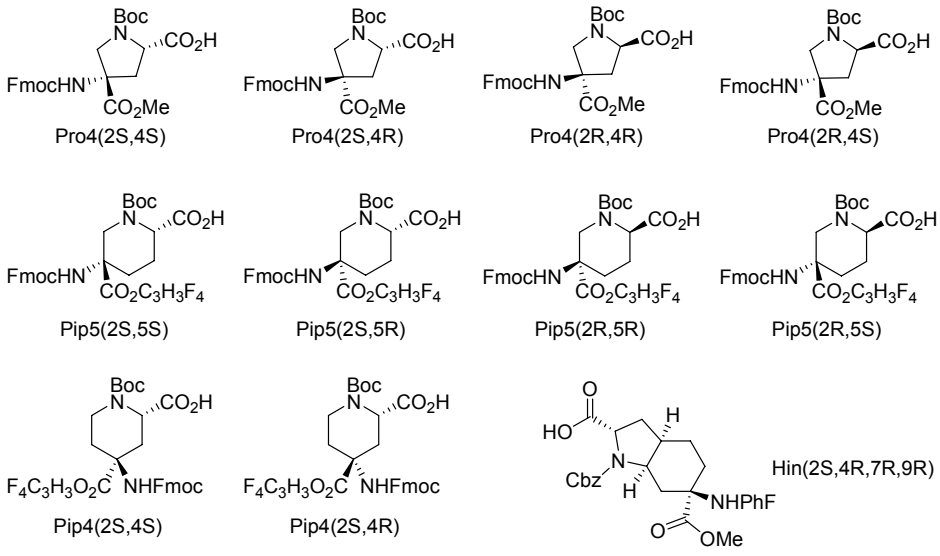

Figure 6. Library of Monomers

Our bis-amino acid monomers[23-27] (Figure 6) are derived from inexpensive, commercially available starting materials. The synthesis of our Pro4(2*S*,4*S*) monomer starts with Cbz-protection of 4-hydroxyproline to provide **2** (Scheme 1**)**. Oxidation to **3** with Jones reagent, and subsequent protection of the carboxylic acid as its corresponding *t*-butylester provided the fully protected 4-ketoproline intermediate (**4**). Application of the Bucherer–Bergs reaction at this stage allowed for access to a mixture of two diastereotopic hydantoins (**5**) that could be conveniently separated by column chromatography. Following global Boc activation to provide **6**, base hydrolysis of the urea revealed the latent amino acid **7**. The resulting primary amine was Fmoc protected to provide (**8**) and the acid converted to its corresponding methylester (**9**) with TMS-diazomethane. Removal of the *t*-butylester with TFA in dichloromethane proceeded to yield **10**, and allowed for the ultimate Cbz to Boc protecting group exchange, and completion of the Pro4(2*S*,4*S*) monomer (**11**) synthesis. Syntheses of the other monomers are analogous to that described in (Scheme 1).

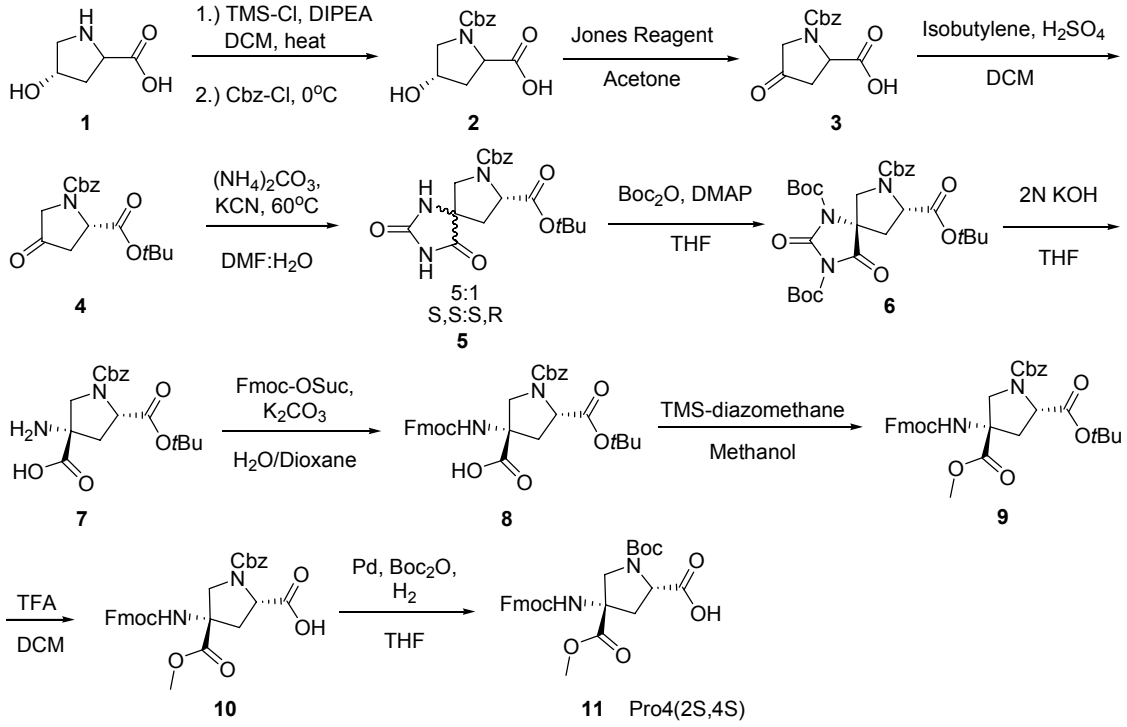

Scheme 1. Synthesis of Pro4(2*S*,4*S*) monomer

Although the Pro4 monomer syntheses were developed previously, we were able to introduce a more reliable method for Fmoc protection in which 9-Fluorenylmethyl succinimide carbonate carbonyl (Fmoc-OSu)[28] was used in place of 9-Fluorenylmethyl chloroformate (Fmoc-Cl) to protect the primary amine. Fmoc-OSu proved to be a superior reagent, providing the protected product in good yield and high purity, in addition the reagent allowed for reduced reaction setup time and cost, and was easily amenable to scale up without compromising product yield.

1.4 BIS-AMINO ACIDS INCORPORATION INTO RIGID A SCAFFOLD

Molecular scaffolds derived from our monomers are assembled using standard Fmoc solid phase peptide synthesis[29]. An advantage of solid phase synthesis is that reactions can be driven to >99% completion in the presence of excess reagents which can be easily removed at the end of the reaction by simple filtration. Our scaffolds are generally synthesized on a polystyrene polymeric support using standard Fmoc peptide synthesis protocols. In order to couple the first residue onto the alcohol which is immobilized onto the solid support, 1-(Mesitylene-2-sulfonyl)-3-nitro-1H-1,2,4-triazole (MSNT) is used to activate the amino acid. Each building block thereafter is coupled to the next using O-(7-Azabenzotriazol-1-yl)-*N*,*N*,*N*',*N*'-tetramethyluroniumhexafluorophosphate (HATU) activation (Scheme 2). Fmoc removal is achieved by treatment with 20% piperidine in DMF for 30 min. Fmoc deprotections were quantified by measuring the UV absorbance of the dibenzylfulvene-piperidine adduct at 301 nM ($\varepsilon = 7800\ cm^{-1}mol^{-1}$). In order to monitor our scaffolds by HPLC following cleavage from the resin, a UV chromophore such as 1-naphthylalanine or tyrosine is incorporated early in the synthesis.

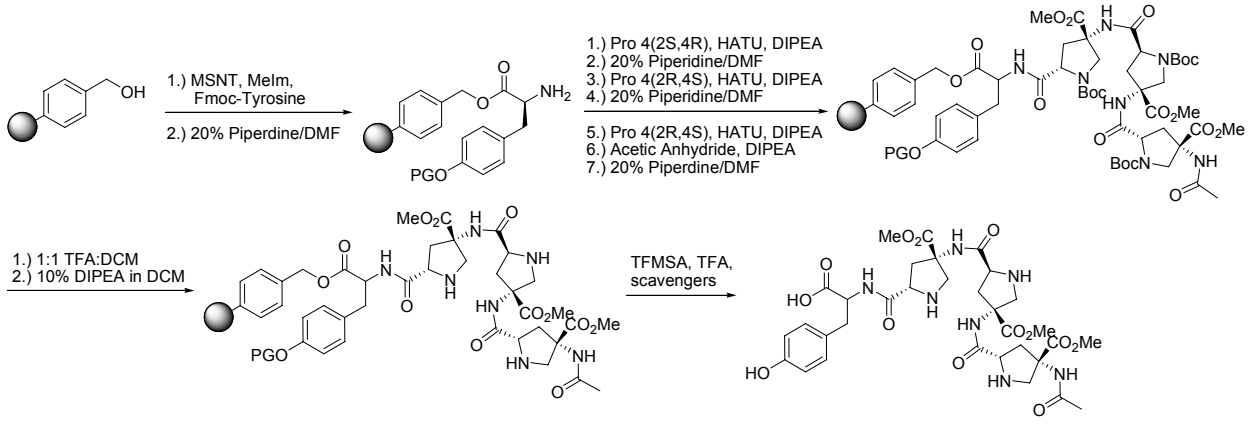

Scheme 2. General synthesis of bis-amino acid scaffold

Once the scaffold is synthesized and cleaved from the resin, multiple diketopiperazines are formed along the scaffold backbone using a solution of 20% piperidine in NMP (Scheme 3). This affords a rigid backbone that provides a novel approach to well-defined molecules that can be synthesized on a relatively short time scale. The completed scaffolds were purified by preparative reverse phase HPLC on C18.

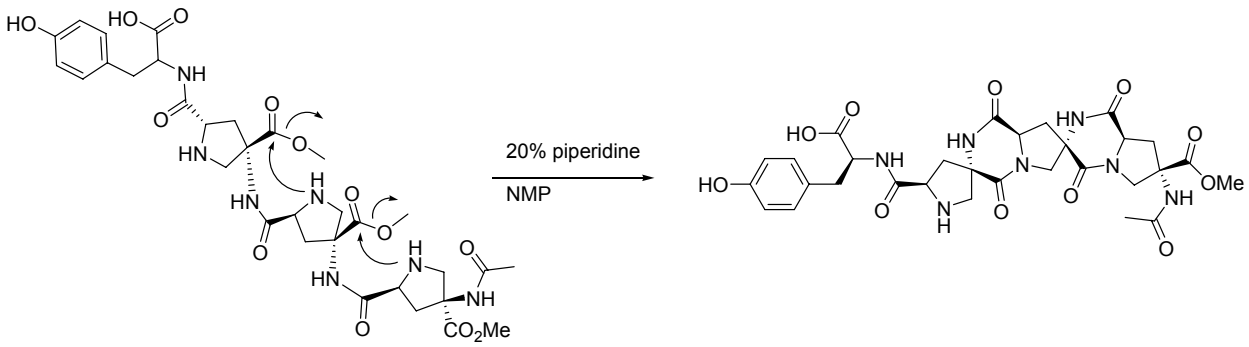

Scheme 3. Diketopiperazine Closure of a Tetramer

The purified materials were subjected to analytical HPLC-MS to assess both molecular weight and purity. From a small set of 10 building blocks, there are 10^4 (10,000) different possible tetramer structures that could be constructed, allowing for an extremely diverse array of rigid structures. Our long-term goal utilizing bis-amino acid monomers is to control overall shape and size of scaffolds that would exhibit the required surface features to accomplish a specific biological task in order to produce useful catalysts, sensors, mini-proteins and various molecular machines.

1.5 MICROWAVE ASSISTED DIKETOPIPERAZINE CLOSURE

Diketopiperazine formation has been the subject of several reviews[30, 31]. Our initial DKP closure conditions employed an intramolecular aminolysis reaction between an amine and an ester catalyzed by 20% piperidine in dimethylformamide. These conditions are quite reliable for producing our rigid scaffolds containing Pro4 monomers, however they are not ideal for several reasons. The major concern under these basic conditions is that epimerization can occur[32] and that these conditions cannot afford rigidified Pip5 scaffolds. This led us to develop mild and general conditions to rigidify all scaffolds.

Utilizing acid catalyzed conditions to close DKPs would potentially allow reaction mixtures to be heated in order to reduce reaction times without endangering the stereocenters. Microwave (MW) irradiation is an attractive approach over traditional heating for several reasons. MW heating provides a more efficient means for heating a reaction mixture. This technique has frequently been demonstrated to produce higher product yields in contrast to the same reaction being carried out under conventional heating. Combining MW irradiation and an acid catalyst could offer an alternative for DKP formation and potentially would improve our approach to rigid scaffolds not only through decreased reaction times, but could allow for more demanding sequences to undergo DKP formation.

Our initial studies were designed to determine if we could utilize acidic conditions in conjunction with microwave heating to close DKPs between Pro4 monomers (Scheme 4). If the conditions indeed worked, we could determine the half-life of DKP closure. We studied several solvents (NMP, DMF, *o*-Xylene), under MW irradiation at several temperatures (70°C, 100°C, 130°C), and in the presence of one catalyst (80mM acetic acid, 80 mM benzoic acid, 50 mM triethylamine and 100mM acetic acid, and 50mM triethylamine and 60mM acetic acid).

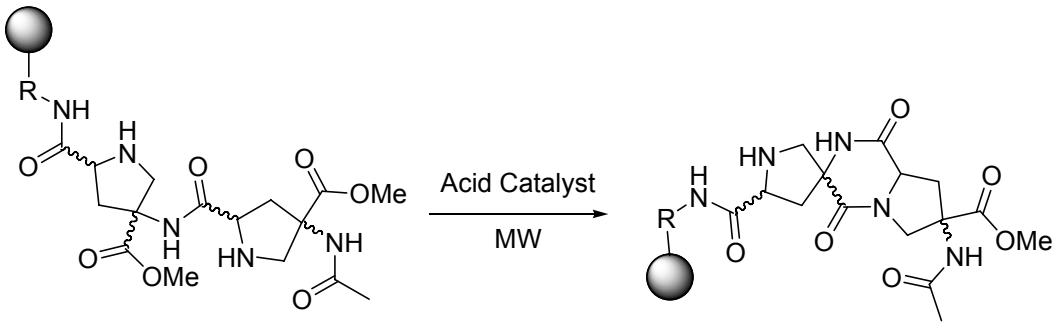

Scheme 4. General DKP closure using acidic conditions

The derivitized resin was heated at the desired temperature and duration inside a CEM Discover microwave. This was repeated over a series of time points. We assumed that this reaction obeys first order kinetics and a plot of ln I [I= area of starting material/ area of starting material + area of product (analyzed by HPLC)] against time *t* seems to support this assumption as it provides a linear fit to the observed data points. From these data we were able to derive the half-life for this transformation given by the equation $t_{1/2}$=ln 2/ k. From Figure 7 a straight line of the data when ln I is plotted against time *t* suggests a half life of 35.4 minutes for the closure of one diketopiperazine under the conditions of 80 mM AcOD at 100 ° C in DMF. We concluded that acidic conditions could effectively close one DKP between Pro4 monomers and drastically reduced reaction time from previous basic conditions.

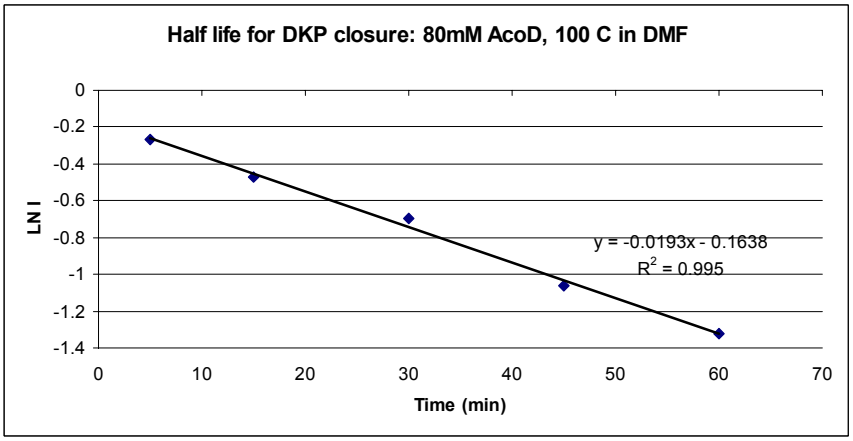

Figure 7. Half-life experiment of DKP closure.

Since the 20% piperidine in DMF was unable to close DKPs between Pip5 monomers we set out to extend the acidic condition to see if they could close DKPs between Pip5 monomers. The acidic conditions under microwave heating could close a DKP between Pip5 monomers, however, the reaction was extremely slow. Sharad Gupta proceeded to develop second generation monomers (Figure 8) in which the methyl ester had been replaced with a 2,2,3,3-tetrafluoropropyl (TFP) esters. This allowed us to examine the effect of the improved leaving group in the TFP ester. Indeed, scaffolds with the TFP ester demonstrated greatly accelerated DKP closure.

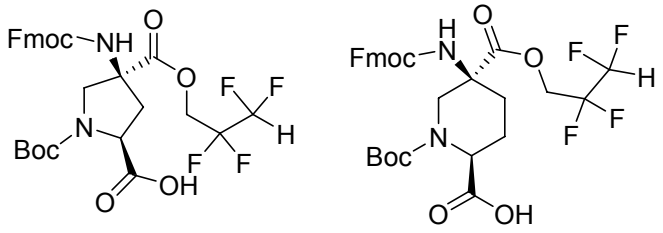

Figure 8. Pro4 and Pip5 TFP ester monomers

The reaction conditions 100mM AcOD, 50 mM TEA, 130° MW for 30 min were employed in closing five DKP between Pip5(2*S*5*S*) (TFP esters) a previously sluggish reaction containing Pip5 methyl ester building blocks, utilizing microwave irradiation (Figure 9).

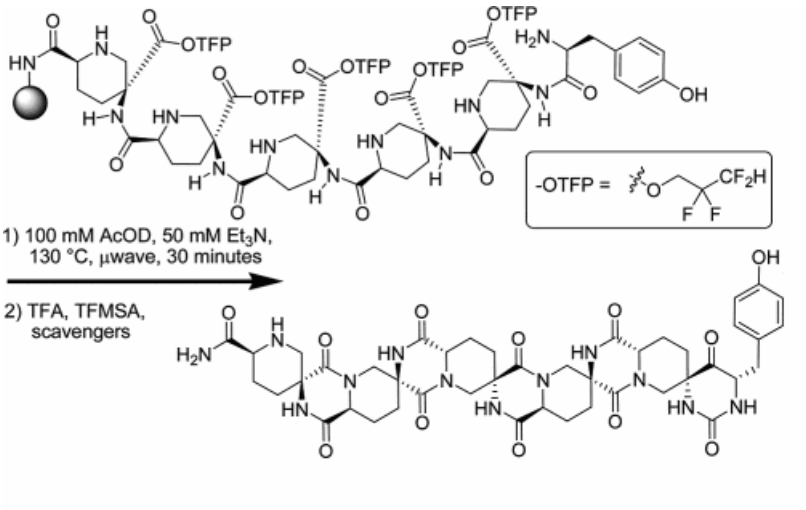

Figure 9. Second-generation monomers undergoing DKP formation

The cleaved product was characterized by C18 reverse-phase HPLC (Figure 10) with mass spectrometry. After 30 minutes the major peak was indicated by mass spectrometry to be the desires product. Two smaller peaks correspond to intermediates that failed to close one DKP. There was no evidence that epimerization occurred.

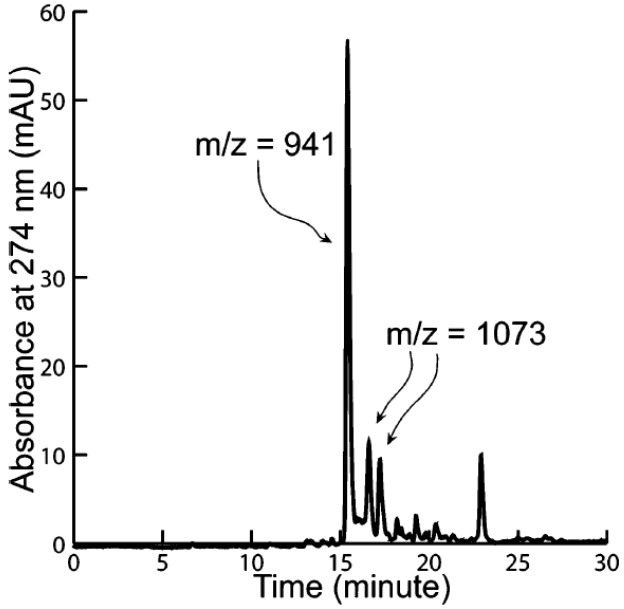

Figure 10. Unpurified reverse-phase C_{18} HPLC of Pip5 scaffold

Recently our work was published[33] and we are currently employing this new methodology to synthesize larger and more complex rigid oliogomers.

1.6 PREVIOUS WORK

Utilizing the unique Computer Aided Nanostructure Design and Optimization (CANDO) software[34], in conjunction with the molecular mechanics package of MOE[35], we were able to predict the probable conformations for our rigid scaffolds. This allowed us to first rapidly screen numerous interesting and unique structures using CANDO, and then synthesize the most interesting structures in the laboratory. Two dimensional NMR spectroscopy techniques were routinely used to confirm that the solution structures of the molecular scaffolds synthesized in the lab correspond with the predicted structures, thus allowing constant evolution and refinement of CANDO. Structure determination was achieved through analysis of the results provided by ^{1}H-^{1}H Correlated Spectroscopy (COSY), ^{1}H-^{13}C (HMQC), long range ^{1}H-^{13}C (HMBC), and through-space ^{1}H-^{1}H (ROESY). For the Pro4 building blocks, key structural information has been previously reported[23, 24]. It has been demonstrated the diketopiperazine between two Pro4 building blocks forms a shallow boat conformation, in which the R_1 substituent resides in a pseudo-equatorial position (Figure 11). An envelope conformation is adopted by the five membered ring to avoid 1,3 diaxial strain between the carbonyl and amide proton. To date no x-ray crystal structures of our scaffolds have been obtained.

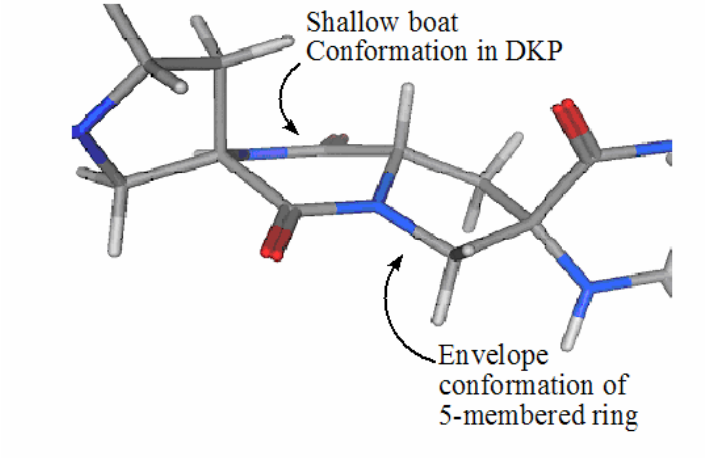

Figure 11. Conformation of the Pro 4 monomer within a scaffold

1.7 SELF ASSEMBLY THROUGH HYDROGEN BONDS

Assembly of molecules through weak non-covalent interactions (i.e. hydrogen bonds) is a phenomena widespread in nature. In a strand of double helical DNA, the base pairs of adenine and thymine, or guanine and cytosine form intermolecular hydrogen bonds that define and rigidify the helical structure of DNA. Developing the ability to control tertiary structure through manipulation of hydrogen bonding, as nucleic acids and proteins are able to, has attracted much attention. Hydrogen bonds are important because of the effects they have on the properties of compounds: boiling point, melting points, solubility, spectral absorption positions. Hydrogen bonding is particularly attractive for the creation of self-assembled molecules because arrays of hydrogen-bond donor and acceptors can be utilized to induce self-assembly and because hydrogen bonds can be directional.

Hydrogen bonding can be detected in many ways. One of the most valuable techniques for assessing these interactions is through is Infrared Spectroscopy (IR). The IR frequencies of common hydrogen bond donor and acceptor, such as O-H or C=O are red shifted when the group

is hydrogen bonded. For example, a free alcohol absorbs at ~3590-3650 cm^{-1}, whereas a hydrogen bonded O-H group absorbs ~50-100 cm^{-1} lower frequency. As seen in Figure 12 (b), a red shifted peak at 3430cm^{-1} corresponds to a hydrogen-bonded NH absorption in a *N*,*N*-bis(2-cyanoethyl)-*N*'-methylurea[19]. In the IR spectra (295 K) (a) at 10 mM the molecule exhibits modest self-association while at 50 mM (b) the molecule exhibits a substantial hydrogen-bonded NH peak.

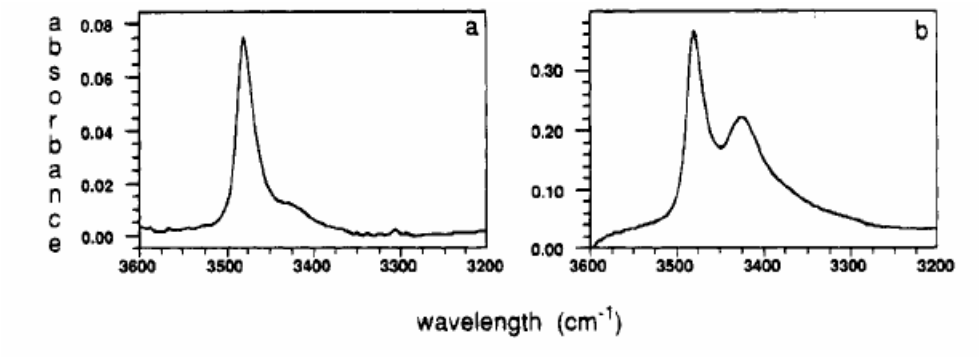

Figure 12. IR spectra of Intramolecular Hydrogen Bonded Ureas. (a) 10 mM: 3481, 3430 cm^{-1} (weak) (b) 50 mM: 3481, 3425 cm^{-1}.

NMR spectroscopy can also be utilized to detect hydrogen-bonded species. Chemical shifts for hydrogen bonded amide protons and non-hydrogen bonded amide protons greatly differ due to the presence of the hydrogen bond. In the presence of a hydrogen bond, shielding effects induced by the acceptor alter the amide proton chemical shift relative to non-hydrogen bonded amide protons. Chemical shifts depend on the inverse third power of the distance between amide proton and hydrogen bond acceptor[36]. As the temperature of the NMR sample is increased, thermal energy of the system increases resulting in an increase in the length of the hydrogen bond. As the length of the hydrogen bond increases, shielding affects arising from the proximity of the hydrogen bond acceptor are dramatically decreased and thus the chemical shift of the amide proton is shifted downfield to a lesser extent.

A complementary experiment to variable temperature NMR is dilution NMR. If a system does self-assemble, the aggregation state will depend on the concentration. At a defined concentration the system will self-assemble, but as the concentration becomes increasingly dilute, the system becomes less likely to associate. An example of this phenomenon demonstrated using the short peptide sequence in Figure 13[37]. Figure 14 describes the concentration study on this molecule performed in $CDCl_3$. The chemical shift of the urea NH is shifted downfield ~0.2 ppm when self-assembled and as the concentration is decreased the urea NH is shifted upfield.

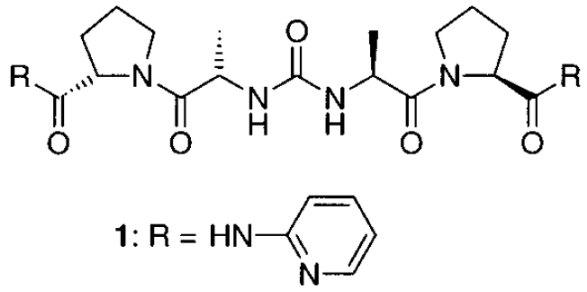

Figure 13. Dipeptidyl Urea

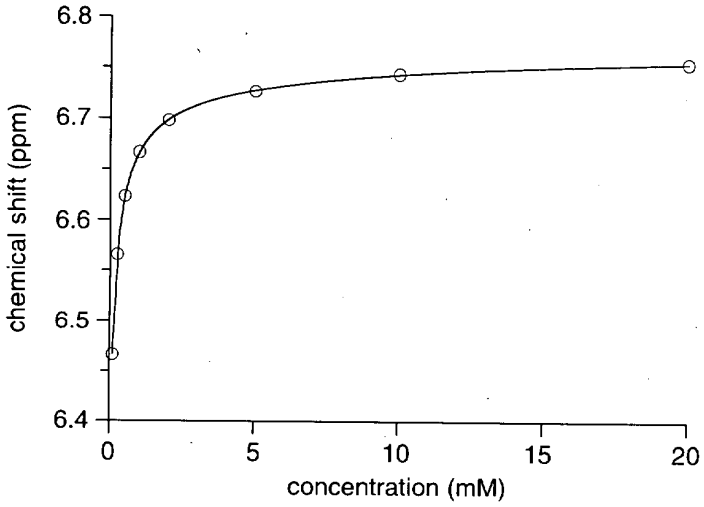

Figure 14. 1H NMR shift of Urea NH at 25 °C in $CDCl_3$.

Another useful NMR phenomenon for detecting self-assembly in solution is the proton magnetic resonance nuclear Overhauser enhancement (nOe). Observation of an nOe of one hydrogen signal on irradiation of another indicates that those hydrogens are within 4 Å of one another. Therefore, if a molecule is interacting with itself, nOe's should be observed from one scaffold to the second scaffold correlating protons in proximity. An nOe experiment was used to confirm that the molecule in Figure 13 was indeed forming higher order structures in solution. The solid arrows indicate the observed NOE's[37].

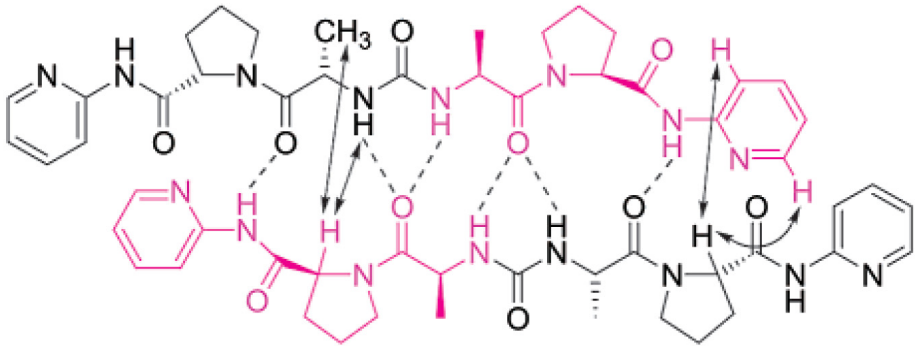

Figure 15. NOE's observed between dipeptidyl ureas.

2.0 BIS-AMINO ACIDS: AN APPROACH TOWARDS SELF ASSEMBLY

The primary focus of my graduate research has been the synthesis of **13** (Scheme 5) and exploring its potential for self-assembly into higher order structures (dimers, trimers, tetramers, etc.). This particular scaffold sequence (**13**) sparked interest because of its apparent potential for aggregation through hydrogen bonded networks. Utilizing CANDO in conjunction with the molecular mechanics package MOE, we have been able to predict with reasonable certainty several probable conformations of **13**. The energy minimized structure of **13** provided by MOE revealed a pair of amide bonds with hydrogen bond donor and acceptor: 4HN and 5O, 2HN and 3O which could potentially participate in the formation of four intermolecular hydrogen bonds along the scaffold's rod-like backbone (Figure 16)

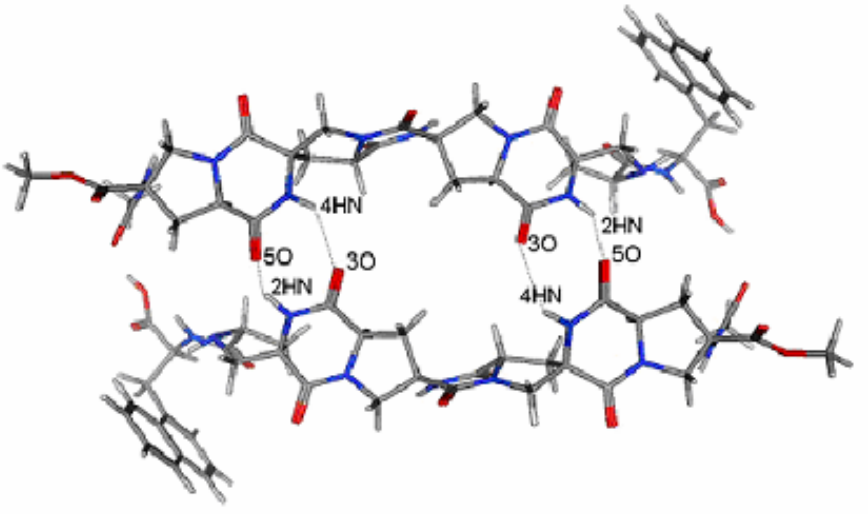

Figure 16. Proposed conformation of self-assembled scaffold 13

2.1 RESULTS

2.1.1 Synthesis of Scaffold

The synthesis of molecule **13** (Scheme 5) was achieved using standard solid phase techniques. The hydroxymethyl resin was chosen as the solid support because of its relatively high loading and facile cleavage in the presence of triflic acid (TfOH). Naphthylalanine was first coupled to the resin to provide a UV chromophore to aid in monitoring the scaffold throughout diketopiperazine (DKP) closure and purification. Naphthylalanine was chosen over the more polar tyrosine because we envisioned that it would aid in improving the solubility of the final product in non-polar, aprotic solvents. The building blocks Pro4(2*S*,4*R*), Pro4(2*R*,4*S*), Pro4(2*S*,4*R*), Pro4(2*R*,4*S*) were then sequentially coupled to the resin. After removal of the final Fmoc group in 20% piperidine in DMF, the free primary amine was acylated using 4mL of a 100:25:2 DMF:Acetic Anhydride:DIPEA solution. Global Boc deprotection was accomplished using 1:1 TFA:DCM. Upon completion of the solid phase synthesis, the resin was dried further under high vacuum to ensure complete removal of residual solvents.

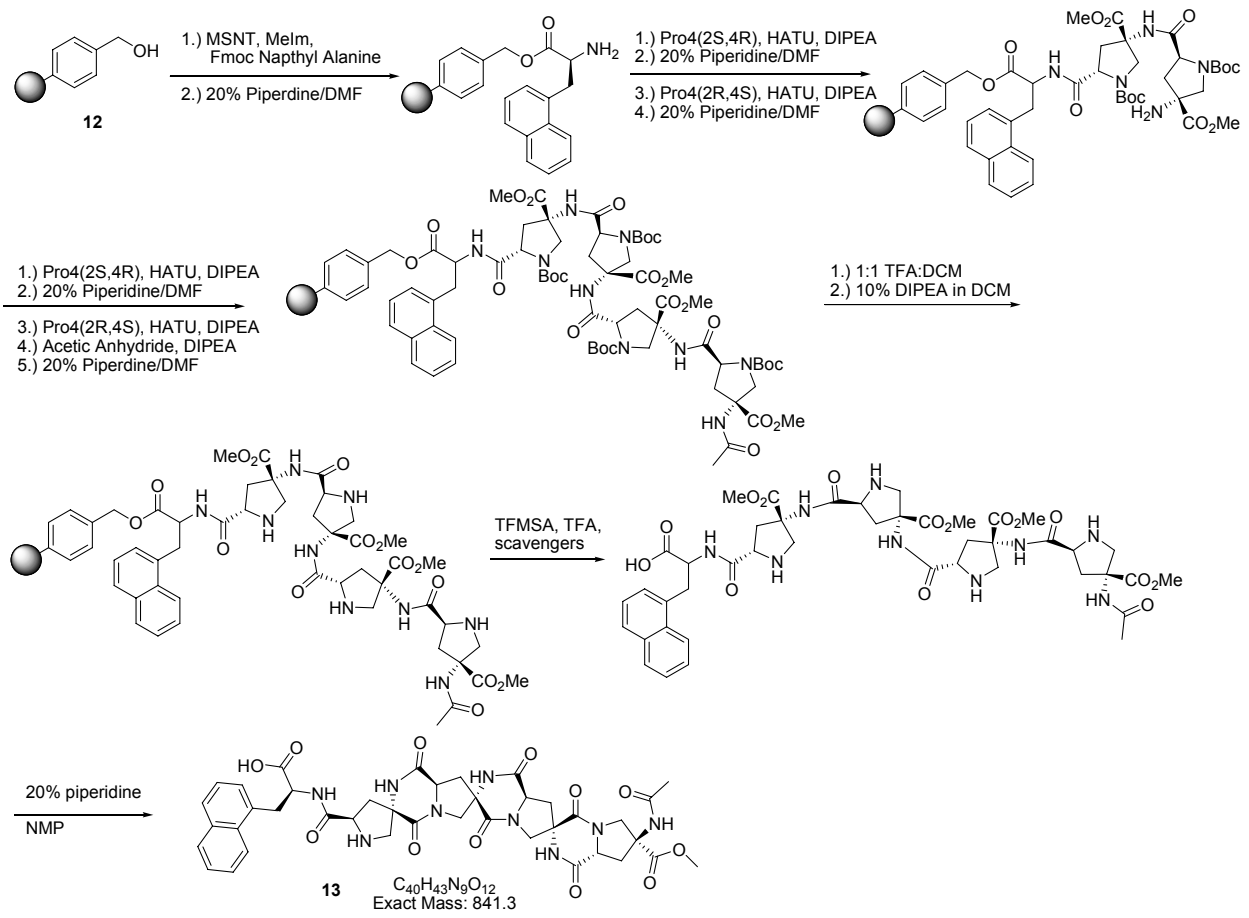

Scheme 5. Solid Phase Synthesis of Scaffold 13

Cleavage of the scaffolds from the hydroxymethyl resin was achieved using standard triflic acid conditions. Once the cleaved product was precipitated into ether, diketopiperazine formation was undertaken in NMP and promoted in the presence of 20% piperidine in NMP over 48 h to yield the rigidified final product **13**. Preparative reverse phase HPLC purification of **13** allowed for the isolation of the desired material in >98% purity (Figure 23).

2.1.2 Solubility of Scaffold

In order to study our molecule designed for self-assembly, multiple solvent systems were explored to identify solubility properties of the scaffold. Ideal solvents are non-hydrogen

bonding solvents such as chloroform, dichloromethane, benzene. Unfortunately molecule **13**, was found to be insoluble in both chloroform and dichloromethane. Using ChemDraw, an estimated log P value (-6.24) was obtained for **13**, indicating that our molecule was extremely polar. Realizing the reason for our scaffolds utter insolubility in nonpolar solvents, our efforts were directed to finding a more polar solvent system in which our molecule would be soluble while hopefully not disrupting the scaffolds ability to undergo self assembly too severely.

In the past, our scaffolds have generally proven to be quite water-soluble. We thought that if our molecule was indeed capable of self-assembly, that it would be possible to detect intermolecular hydrogen bonding in water, despite the interference of water on this interaction. However, the scaffold of interest (**13**) was not soluble in H_2O. Even at pH 3.5 ammonium acetate buffer (90% H_2O:10% D_2O) the scaffold was insoluble. However, upon addition of an aqueous solution containing 0.2 % TFA the molecule was adequately dissolved. It is likely that the addition of TFA was suppressing or destroying the very interactions we hoped to study, breaking apart any higher order structures, and ultimately allowing the scaffold to dissolve. Nonetheless, we then decided to continue the search for a solvent system that would better allow us explore the self-assembly of molecule **13**. Exploration of self-assembly in H_2O would require solvent suppression NMR in order to see the chemical shifts of the amide protons. Acetonitrile was an appealing solvent due to its polarity and it's poor capability for the formation of hydrogen bonds. However, once again, our molecule was insoluble in this solvent. Acetone and methanol were also explored, however both solvents failed to dissolve our scaffold. It was later determined that molecule **13** was soluble in DMSO.

2.1.3 Variable Temperature NMR Experiments

Our first attempt to detect intermolecular hydrogen bonds between individual scaffolds was designed around a variable temperature NMR experiment. We hoped to see if any notable, nonlinear changes in chemical shift of the scaffold's amide protons would occur upon heating. Initially, our experiment was performed with scaffold concentrations of 13 mM in $DMSO_{d6}$ containing 0.2% TFA. Figure 17 provides the results from this experiment. A linear relationship between the amide proton chemical shifts and temperature for all five amide protons was observed. As the temperature dependence of proton chemical shifts of intermolecularly hydrogen bonded amides should differ greatly from those amides not involved in hydrogen bonding, we interpreted our result as not supportive of our initial hypothesis for self-assembly in the selected solvent system. The variable temperature NMR experiment was repeated at two different scaffold concentrations: 4mM, and 1mM. We anticipated that if self-assembly was occurring, its effect on amide bond chemical shifts would demonstrate a concentration dependence. Unfortunately, results from these additional experiments provided a similar linear relationship of chemical shifts with respect to temperature for all five nitrogen amide protons (Figure 18, Figure 19). These findings did not support the hypothesis of intermolecular hydrogen bonding under the conditions employed.

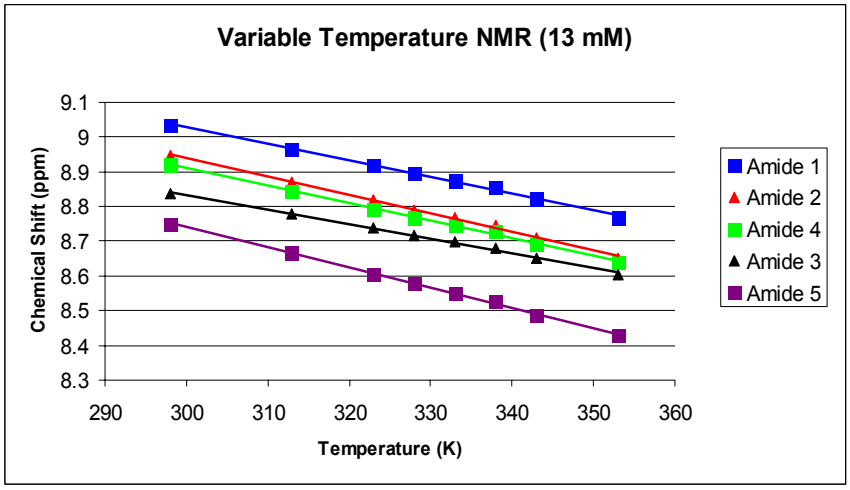

Figure 17. Variable Temperature NMR Experiment (13mM)

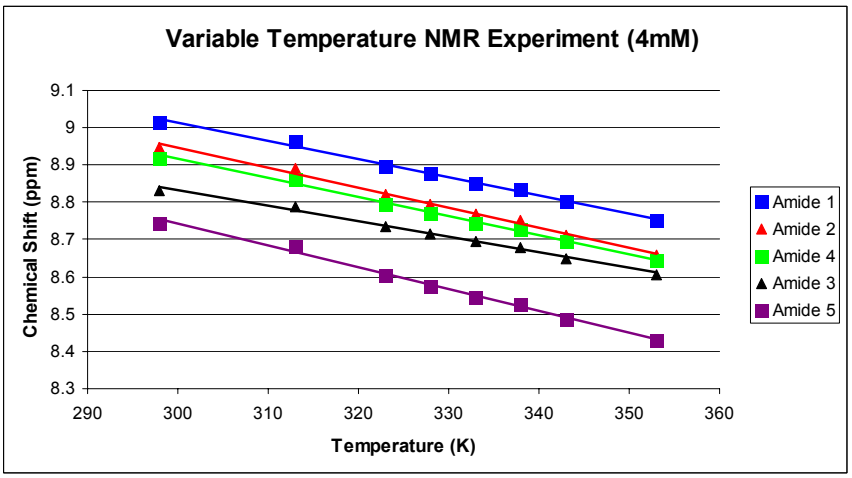

Figure 18. Variable Temperature NMR Experiment (4mM)

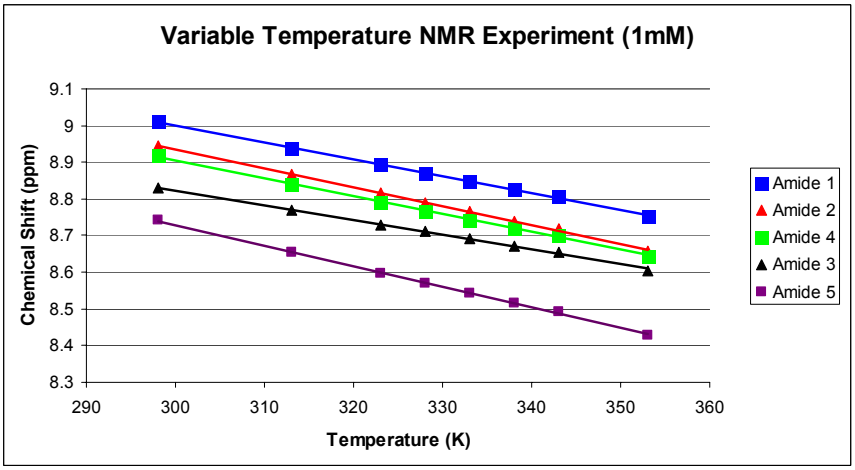

Figure 19. Variable Temperature NMR Experiment (1mM)

2.1.4 Structural Characterization of Scaffold

Full structural characterization of the scaffold was the next logical step to ensure that the molecule under study was indeed what we had set out to synthesize. From the 2D NMR data we were able to discern the overall shape of our scaffold, and compare it with those structures predicted initially by CANDO. Our scaffold was quite similar to the predicted structures as evidence by superimposing the observed COSY, HMQC, HMBC, and ROESY correlations onto the energy minimized conformation generated by MOE (Figure 21). Structural characterization was completed at a substrate concentration of 13mM in $DMSO_{d6}$ containing 0.2% TFA. The 2D NMR spectra were assigned using the graphical NMR assignment and integration program SPARKY. The NMR data confirmed the expected connectivity and stereochemistry of the scaffold (Figure 21).

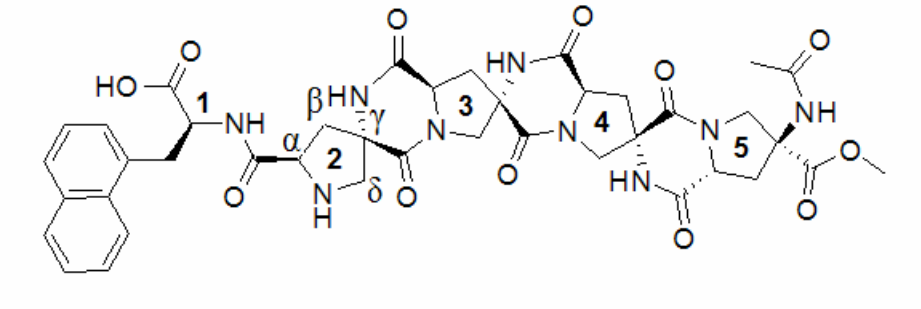

Figure 20. Nomenclature for Structural Characterization

The next section does not attempt to explain every correlation from each NMR experiment as that would be tedious to read and understand. The following is only intended to serve as an example of how many of the assignments were made.

From the COSY experiment, each alpha proton was coupled to the corresponding beta protons. (See Figure 16 for nomenclature of the scaffold). The HMQC correlated protons to the carbon atoms they were attached. The HMBC correlated long range couplings between (two and three bonds) proton to carbon atoms allowing for assignments within each Pro4 ring to be made. For example, the carbon atom at the beta position was correlated to the alpha proton and the carbon atom at the gamma position was correlated to the beta proton. Two valuable assignments from the HMBC were the observed correlations between the ester carbonyl of the fifth residue to the isolated methyl group, and a correlation between the carbonyl of the acetyl moiety of the fifth residue to its neighboring methyl protons. These protons were easily differentiated from other protons in the scaffold by their ^{1}H NMR integrals, and were easily differentiated from one another through differences in their observed chemical shifts. The ester protons were shifted downfield at ~3.5 ppm compared to the acetamide which resonates at ~1.8 ppm. Once these assignments were made, it allowed other assignments from the HMBC to follow.

Working from the other end of the molecule, the carbonyl of the carboxylic acid was assigned through HMBC correlation with the alpha and beta protons of the naphthylalanine (first) residue. Also the chemical shift of the carbonyl (farthest downfield) supported the assignment. Other important assignments within the proline rings were correlations between the alpha carbon to the amide of the previous residue (across DKP). For example, the alpha carbon of the third residue was correlated to the amide proton of the second residue. Amide protons were also correlated to both carbonyl carbons of the DKPs.

For spatial assignment, the ROESY data was able to correlate neighboring protons residing on the same face of the scaffold (pseudo axial vs. pseudo equatorial). For example, the

alpha protons are coupled through space to only one beta and one delta proton, as these protons reside are the same face of the proline ring.

2.1.5 ROESY Data

Correlations between protons were differentiated by peak intensity. Intensities were classified as strong (red), medium (green), and weak (blue). From the NMR analysis we were certain that the connectivity of our molecule was indeed as we expected it to be and that the rod-like shape that we initially proposed was indeed present. A key correlation (not shown) was 2HB1 to 3NH which provides further evidence of the rod-like backbone. If self-assembly was indeed occurring within our scaffold through the proposed pair of amide bonds, then we expect to observe ROESY correlations between an amide proton and a remote proton that could only arise through intermolecular hydrogen bonding. Unfortunately, ROESY analysis failed to produce any signals of this type, consistent with the absence of self assembled networks in solution.

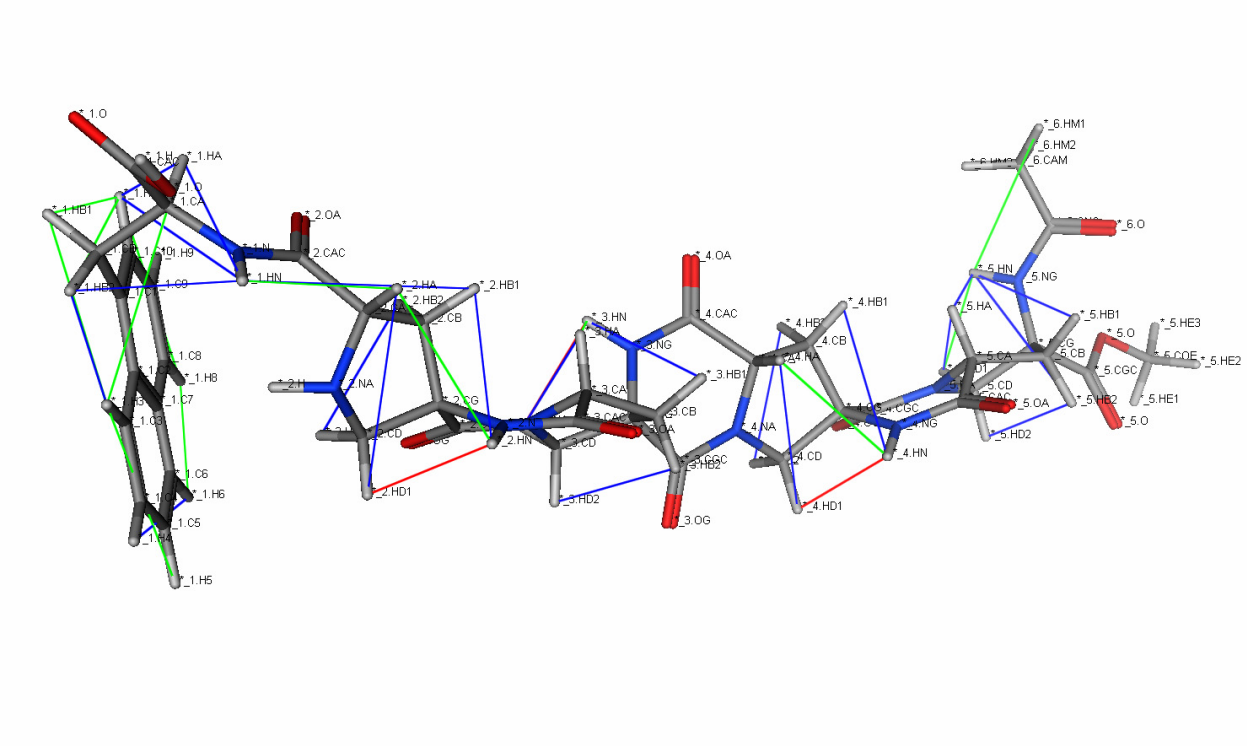

Figure 21. ROESY correlations superimposed onto the energy minimized structure

Under the initial conditions employed, we were not able to produce any evidence that suggested our system was behaving as it was originally designed. We then turned our efforts towards a competitive solvent experiment. Our thought was that by titrating a non-polar solvent into our sample would effect a change to the overall polarity of the system and would hopefully facilitate the formation of intermolecular, hydrogen-bonded networks. We were curious to see what we would observe in the amide proton chemical shifts as the solvent environment would become more and more nonpolar. DCM_{d2} was titrated to an original solution of 5.6 mM of our sample dissolved in 20% DCM_{d2} in $DMSO_{d6}$. A ^{1}H NMR was taken after each addition of DCM_{d2} (decrease concentration by 0.1 mM – 0.3 mM) and the amide proton chemical shifts were observed. Our scaffold remained soluble even at 0.7mM in 90% DCM_{d2} in $DMSO_{d6}$. Although the amide chemical shifts were changing upon addition of DCM, the trend was not

obvious. The amide protons on the C-terminus and N-terminus residues were changing more rapidly than those on the interior of the molecule, possibly suggesting that our molecule was not assembling as it was initially designed, but that the exterior residues were promoting aggregation under the experimental conditions. The NMR sample was left overnight at 0.7mM in 90% DCM_{d2} in $DMSO_{d6}$ and molecule **13** precipitated. A ^{1}H NMR was taken of the sample with precipitate and its chemical shifts were identical to the previous sample without precipitate. This suggested that the need for additional data points at higher concentration of DCM_{d2} were unnecessary.

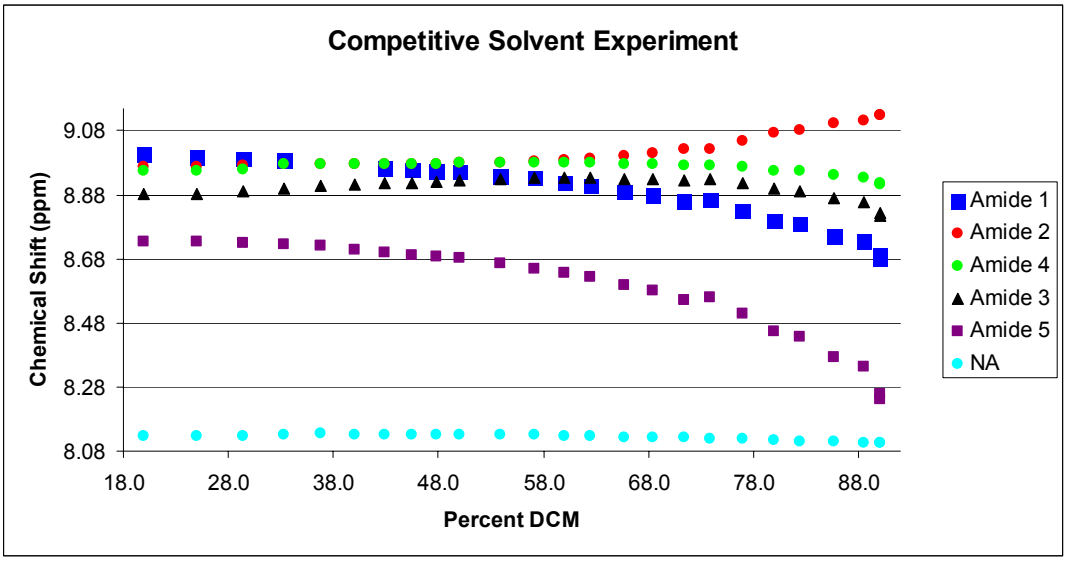

Figure 22. Competitive Solvent Experiment

2.2 CONCLUSION

Scaffold **13** (napthylalanine-Pro4(2*S*4*R*)-Pro4(*2R*4*S*)-Pro4(2*S*4*R*)-Pro4(2*R*4*S*)) was successfully synthesized using standard Fmoc Solid Phase Peptide Synthesis. Full structural characterization (^{1}H NMR, COSY, HMQC, HMBC, ROESY) confirmed desired connectivity. Scaffold **13** was probed for its ability to self-assemble in $DMSO_{d6}$ in the presence of 0.2 % TFA (13 mM – 4 mM). Scaffold **13** did not support our hypothesis for self-assembly under any of the conditions explored. ROESY correlations failed to indicate self-assembly between interacting scaffolds and a variable temperature (25 to 80 °C) NMR study at three separate concentrations (13 mM, 4mM, 1 mM) also failed to produce results to support the notion of self-assembly.

The sequence selected was based on models generated from CANDO. Perhaps the driving force for self-assembly in our molecule was too strong and led to the scaffolds utterly insolubility in non-polar solvents. It is possible that the actual solution structure of the scaffold precluded its ability to self-assemble. As we continue to gather structural knowledge about our scaffolds, while iteratively improving our modeling techniques, a sequence better suited for self-assembly may emerge. Additional building blocks from our toolbox may need to be incorporated into the sequence of interest, especially an emerging, functionalized building block that could potentially allow for additional side chain interactions. It may be possible that the sequence selected did not provide a large enough driving force, enough hydrogen bonds between the scaffolds, to facilitate self assembly; or perhaps unforeseen steric or electronic factors were working against us. A longer sequence would increase the number of hydrogen bonds between the scaffolds and may in turn provide the appropriate driving force for the scaffold to self-assembly.

2.3 EXPERIMENTAL

2.3.1 General Procedure

HPLC-MS analysis was performed on a Hewlett-Packard Series 1050 instrument with diode array detector, Agilent 1100 series LC-MSD SL detector (ES ion source) using a Waters XTerra MS C_{18} column (3.5 μm packing, 4.6 mm x 100 mm). Preparative HPLC was performed on a Varian ProStar 500 HPLC instrument with a Waters XTerra Prep MS C_{18} column (5 μm packing, 30 mm x 100 mm). NMR experiments were performed on either a 500 MHz or 600 MHz Bruker instrument. The spectrum was referenced to DMSO-*d6* at δ_H 2.49 and δ_C 39.5.

Solid phase synthesis was carried out manually using a setup constructed from standard laboratory materials. Dichloromethane (CH_2Cl_2) was distilled from CaH_2 under nitrogen. Anhydrous Dimethylformamide (DMF) was purchased from Aldrich. Diisopropylethylamine (DIPEA) was distilled under nitrogen sequentially from ninhydrin and potassium hydroxide and stored over 4 Å molecular sieves. Fmoc deprotections were determined quantitatively by measuring the absorbance of the dibenzofulvene-piperidine adduct (λ_{max} = 301 nm, ε = 7800 M^{-1} cm^{-1}). (*S*)-*N*-Fmoc-1-Naphthylalanine (95%, 98% *ee*) was purchased from Acros and Hydroxylmethyl polystyrene (100-200 mesh 1% divinylbenzene (DVB) resin was purchased from Novabiochem. MSNT (1-(Mesitylene-2-sulfonyl)-3-nitro-1H-1,2,4-triazole) was purchased from Acros. Pro-4 monomers were synthesized in house according to published procedures[23, 24].

2.3.2 Synthesis of Scaffold

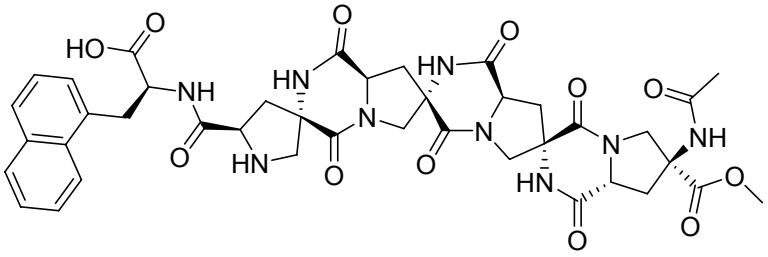

Coupling (*S*)-*N*-Fmoc-1-Naphthylalanine: 50.0 mg Hydroxymethyl resin cross linked with 1% DVB was swollen in DCM for 30 min under an argon atmosphere. Methyl imidazole (MeIm) (20.6 µL, 184 µmole, 3.75 eq.) was added to a 0.2 M solution of (*S*)-*N*-Fmoc-1-Naphthylalanine (107 mg, 245 µmole, 5 eq.) in dry DCM. To this solution was added to MSNT (73 mg, 245 µmole, 5 eq.) and the mixture was allowed to preactivate for 10 min. The coupling solution was added to the resin and agitated under argon for 1 h. Unreacted resin was capped with two successive 4 mL treatments of a 100:25:2 solution of DMF, acetic anhydride, DIPEA for 10 min. The capping solution was drained and the resin was rinsed repeatedly with DMF to remove excess reagents. Fmoc deprotection was achieved by treatment for 30 min with 3 mL of a 20% solution of piperdine in DMF. The progress of the Fmoc deprotection was quantified by aliquoting 10 µL of the 20% piperidine DMF solution bathing the resin beads and diluting to 1mL with an additional quantity of 20% piperidine in DMF. The deprotecting solution was drained and the resin was washed with DMF (2 mL), IPA (2 mL), DMF (2 mL). The resin was then swollen in DMF for 10 min.

Coupling Fmoc-Pro4(2*S*,4R): DIPEA (34.1 µL, 196 µmole, 4 eq.) was added to a 0.2 M solution of Fmoc-Pro4(2*S*, 4*R*) (50 mg, 98 µmole, 2 eq.) in dry DCM in DMF with HATU (37.3 mg, 98 µmole, 2 eq.). This solution was allowed to preactivate for 10 min. The coupling solution was then added to the resin and agitated under argon for 30 min. A second coupling of

Fmoc-Pro 4 (2*S*, 4*R*) was repeated using above procedure. Unreacted resin was capped with two successive 4 mL treatments of a 400:100:8 solution of DMF, acetic anhydride, DIPEA for 10 min. The capping solution was drained and the resin was rinsed repeatedly with DMF to remove excess reagents. Fmoc deprotection was achieved by treatment for 30 min with 3 mL of a 20% solution of piperdine in DMF. The progress of the Fmoc deprotection was quantified by aliquoting 10 μL of the 20% piperidine DMF solution bathing the resin beads and diluting to 1mL with an additional quantity of 20% piperidine in DMF. The deprotecting solution was drained and the resin was washed with DMF (2 mL), IPA (2 mL), DMF (2 mL). The resin was then swollen in DMF for 10 min.

Coupling Fmoc-Pro4(2*R*, 4*S*): DIPEA (34.1 μL, 196 μmole, 4 eq.) was added to a 0.2 M solution of Fmoc-Pro 4 (2*R*, 4*S*) (50 mg, 98 μmole, 2 eq.) in dry DCM in DMF with HATU (37.3 mg, 98 μmole, 2 eq.). This solution was allowed to preactivate for 10 min. The coupling solution was then added to the resin and agitated under argon for 30 min. A second coupling of Fmoc-Pro 4 (2*R*, 4*S*) was repeated using above procedure. Unreacted resin was capped with two successive 4 mL treatments of a 400:100:8 solution of DMF, acetic anhydride, DIPEA for 10 min. The capping solution was drained and the resin was rinsed repeatedly with DMF to remove excess reagents. Fmoc deprotection was achieved by treatment for 30 min with 3 mL of a 20% solution of piperdine in DMF. The progress of the Fmoc deprotection was quantified by aliquoting 10 μL of the 20% piperidine DMF solution bathing the resin beads and diluting to 1mL with an additional quantity of 20% piperidine in DMF. The deprotecting solution was drained and the resin was washed with DMF (2 mL), IPA (2 mL), DMF (2 mL). The resin was then swollen in DMF for 10 min.

Coupling Fmoc-Pro4(2*S*, 4*R*): DIPEA (34.1 µL, 196 µmole, 4 eq.) was added to a 0.2 M solution of Fmoc-Pro 4 (2*SR*, 4*RS*) (50 mg, 98 µmole, 2 eq.) in dry DCM in DMF with HATU (37.3 mg, 98 µmole, 2 eq.). This solution was allowed to preactivate for 10 min. The coupling solution was then added to the resin and agitated under argon for 30 min. A second coupling of Fmoc-Pro 4 (2*S*, 4*R*) was repeated using above procedure. Unreacted resin was capped with two successive 4 mL treatments of a 400:100:8 solution of DMF, acetic anhydride, DIPEA for 10 min. The capping solution was drained and the resin was rinsed repeatedly with DMF to remove excess reagents. Fmoc deprotection was achieved by treatment for 30 min with 3 mL of a 20% solution of piperdine in DMF. The progress of the Fmoc deprotection was quantified by aliquoting 10 µL of the 20% piperidine DMF solution bathing the resin beads and diluting to 1mL with an additional quantity of 20% piperidine in DMF. The deprotecting solution was drained and the resin was washed with DMF (2 mL), IPA (2 mL), DMF (2 mL). The resin was then swollen in DMF for 10 min.

Coupling Fmoc-Pro4(2*R*, 4*S*): DIPEA (34.1 µL, 196 µmole, 4 eq.) was added to a 0.2 M solution of Fmoc-Pro 4 (2*R*, 4*S*) (50 mg, 98 µmole, 2 eq.) in dry DCM in DMF with HATU (37.3 mg, 98 µmole, 2 eq.). This solution was allowed to preactivate for 10 min. The coupling solution was then added to the resin and agitated under argon for 30 min. A second coupling of Fmoc-Pro 4 (2*R*, 4*S*) was repeated using above procedure. Fmoc deprotection was achieved by treatment for 30 min with 3 mL of a 20% solution of piperdine in DMF. The progress of the Fmoc deprotection was quantified by aliquoting 10 µL of the 20% piperidine DMF solution bathing the resin beads and diluting to 1mL with an additional quantity of 20% piperidine in DMF. The deprotecting solution was drained and the resin was washed with DMF (2 mL), IPA (2 mL), DMF (2 mL). Unreacted resin was capped with two successive 4 mL treatments of a

400:100:8 solution of DMF, acetic aanhydride, DIPEA for 10 min. The capping solution was drained and the resin was rinsed repeatedly with DMF to remove excess reagents. Global Boc deprotection was achieved with two successive 2mL treatments of 1:1 solution of DCM:TFA for 10 min. The resin was then swollen in DCM for 10 min. The solution was drained and the resin was rinsed with DMF (2 mL), IPA (2 mL), DMF (2 mL) alternating followed by DCM (2 mL), IPA (2mL), DCM (2 mL) alternating and then swelled in DCM for 5 min. Scaffold was placed under high vacuum overnight to removal residual solvents.

2.3.3 Cleavage from Resin

Ethanedithiol (EDT) (12.5 μL, 0. 149 mmol) and thioanisole (25 μL, 0. 213 mmol) was added to the resin reactor. The reactor was chilled to 0 °C using an ice bath and then trifluoroacetic acid (TFA) (250 μL, 3.35 mmol) was added and the mixture was allowed to stir for an additional 5 min at 0 °C. Trifluoromethanesulfonic acid (TFMSA) (25 μL, 0.282 mmol) was added and the solution was vigorously stirred for 1 hour at 0 °C, followed by an additional 1 h at room temperature. The acidic cleavage solution was drained into 5 mL diethylether. The resin was washed with 3 * 500 μL TFA and the washes were drained into the diethylether solution. The collected material was centrifuged and the solution was decanted leaving a white precipitate. The precipitate was dissolved in 2 mL of a solution containing 74.5% H_20, 25% ACN, and 0.5 % Formic Acid. The sample was subjected to HPLC-MS analysis to check for purity and mass. The sample was eluted from the column using a gradient of 0-50% ACN in H_2O containing 1% Formic Acid over 30 min. The analysis indicated that the isolated material (t_r 12.36 min) was roughly 73 % pure and provided an ion at 937.4 ($M + H^+$), 469.4 ($M + 2H^+$),

313.4 ($M + 3H^+$) m/z consistent with the presence of the desired product. Sample was lyophilized to afford a white powder.

2.3.4 Diketopiperazine Closure

Cleavage product was subjected to 1 mL of dry 20% piperidine in NMP (N-methylpyrrolidone). After 1.5 days the reaction solution was precipitated into cold ether (10 mL). The collected material was centrifuged and the solution was decanted leaving a white precipitate. The precipitate was dissolved in 74.5% H_20, 25% ACN, and 0.5 % Formic Acid. The sample was subjected to HPLC-MS analysis to check for purity and mass. The sample was eluted from the column using a gradient of 0-50% ACN in H_2O containing 1% Formic Acid over 30 min. The analysis indicated that the isolated material (t_r 17.06 min) was roughly 72 % pure and provided an ion at 842.1 ($M + H^+$), 421.6 ($M + 2H^+$) m/z consistent with the presence of the desired product.

2.3.5 Preparative Purification

Preparative purification of the rigidified product was accomplished using a gradient of 0-50% ACN in H_2O containing 1% Formic Acid over 30 min. Fractions containing the desired product were combined and lyophilized to afford a white powder. The purified product was dissolved in 4 mL 74.5% H_20, 25% ACN, and 0.5 % Formic Acid (Figure 23). Product concentration was calculated based upon UV absorbance at 274 nm using a calibration curve of 1-naphthylalanine.

2.3.6 NMR Sample Preparation

(13 mM): The NMR sample of **13** was prepared by dissolving 4.8 μmole of **13** in 369 μL $DMSO_{d6}$ with 0.2% TFA and transferred to a Shigemi NMR tube to afford a 13mM sample. The chemical shift assignments are based upon COSY, HMQC, HMBC, and ROESY correlations. Sparky was used to assign and integrate the 2D spectra.

(4mM): The NMR sample of compound **13** that was used for structural determination (13 mM in DMSO-*d6* with 0.2% TFA) was diluted with 1mL 74.5% H_2O, 25% ACN, and 0.5 % Formic Acid, and purified by preparative HPLC. Prep purification of samples was accomplished using a 0-50% ACN in H_2O containing 1% Formic Acid over 30 min. Fractions containing the desired product were combined and lyophilized to afford a white powder. Product was dissolved in 4 mL 74.5% H_20, 25% ACN, and 0.5 % Formic Acid. Product concentration was calculated based upon UV absorbance at 274 nm using a calibration curve of 1-naphthylalanine. HPLC-MS was used to check for purity and mass using a 30 min 0% ACN to 50% ACN with H_2O and 1% Formic Acid. Sample was freeze dried to afford a white powder. 1.5μ L TFA was added to 750 uL $DMSO_{d6}$. Compound **13** was dissolved in 380 μL $DMSO_{d6}$ with 0.2% TFA and transferred to a Shigemi NMR tube to afford a 4mM sample.

(1mM): The 4mM sample of compound **13** was diluted using 0.2% TFA in 752 μL $DMSO_{d6}$ to afford a 1mM sample.

Competitive Solvent Experiment: The NMR sample of # was prepared by dissolving 2.1 μmole **13** in 300 μL $DMSO_{d6}$ with 0.2% TFA and transferred to a Shigemi NMR tube and then added 75 μL DCM_{d2} to afford a 5.6 mM sample. Each subsequent NMR sample was prepared by titrating in the desired amount of DCM_{d2}Table 1.

Table 1. Competitive Titration Experiment

	Total Volume (uL)	Volume DCM (uL)	DCM Added (uL)	Volume DMSO (uL)	% DCM	mM
1	375	75	-	300	20.0	5.6
2	400	100	25	300	25.0	5.3
3	425	125	25	300	29.4	5.0
4	450	150	25	300	33.3	4.7
5	475	175	25	300	36.8	4.4
6	500	200	25	300	40.0	4.2
7	525	225	25	300	42.9	4.0
8	550	250	25	300	45.5	3.8
9	575	275	25	300	47.8	3.7
10	600	300	25	300	50.0	3.5
11	650	350	50	300	53.8	3.2
12	700	400	50	300	57.1	3.0
13	750	450	50	300	60.0	2.8
14	800	500	50	300	62.5	2.6
15	875	575	75	300	65.7	2.4
16	950	650	75	300	68.4	2.2
17	1050	750	100	300	71.4	2.0
19	1150	850	100	300	73.9	1.8
20	1300	1000	150	300	76.9	1.6
21	1500	1200	200	300	80.0	1.4
22	1700	1400	200	300	82.4	1.2
23	2100	1800	400	300	85.7	1.0
24	2600	2300	500	300	88.5	0.8
25	3000	2700	400	300	90.0	0.7
26	3000	2700	400	300	90	0.7

APPENDIX A

SUPPLEMENTAL DATA

A.1 HPLC DATA

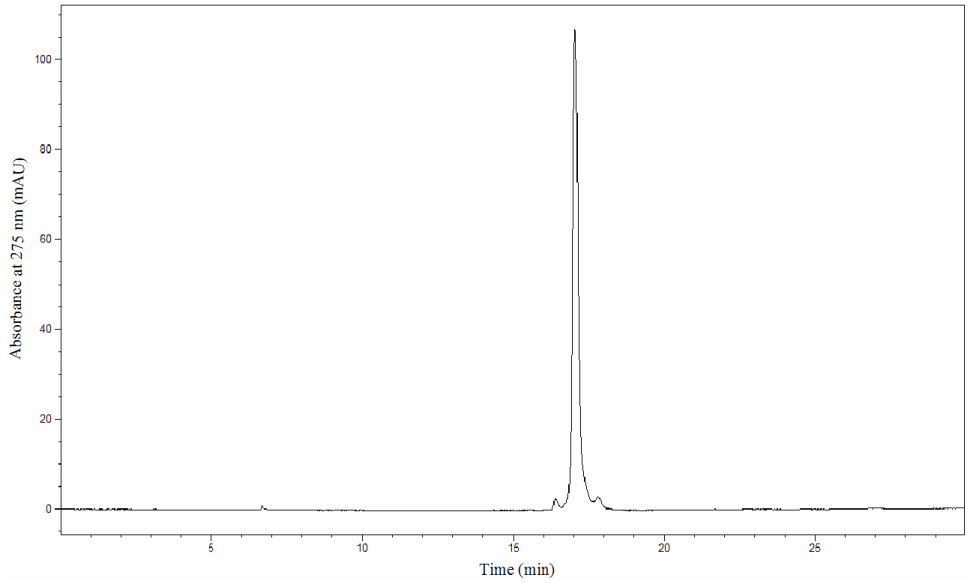

Figure 23. HPLC-MS of Scaffold: mobile phase, H_2O (0.1 % HCOOH) to 50% MeCN (0.05% HCOOH) and 50% H_2O (0.1 % HCOOH over 30 min; flow rate 0.80 mL/min; UV detection at 274 nm; t_r for compound 13, 17.02 min; ESI-MS m/z (ion): 842.2 ($M + H^+$), 421.8 ($M + 2H^+$).

A.2 2 D NMR DATA

Nomenclature in the 2D-NMR data tables:

Residue: the number corresponds to the placement of the residue within the scaffold starting with 1 which corresponds to the C-terminus (napthylalanine)

Atom: refers to the nucleus (C or H) whose chemical shift and correlation is being observed

Position: refers to the location of the nucleus of interest

A = alpha

B = beta

G = gamma

D = delta

N = amide nitrogen

GC = carbonyl carbon adjacent to gamma carbon

CAC = carbonyl carbon adjacent to alpha carbon

C# = carbon off residue 1

H# = hydrogen off residue 1

COE = carbonyl carbon adjacent to the methyl ester

CNC = carbonyl carbon of the acetamide moiety

CAM = carbon of the methyl protons

Table 2. Resonance Assignments for Scaffold

Group	Position	Atom	Chemical Shift	Std Dev	Assignments
1	C1	13C	131.201	0.027	4
1	C10	13C	127.458	0.254	3
1	C2	13C	133.642	0.000	0
1	C3	13C	123.153	0.299	3
1	C4	13C	126.066	0.000	1
1	C5	13C	125.463	0.000	1
1	C6	13C	128.374	0.000	1
1	C7	13C	133.642	0.072	3
1	C8	13C	127.341	0.000	1
1	C9	13C	125.032	0.000	1
1	CA	13C	53.178	0.000	4
1	CAC	13C	172.326	0.048	3
1	CB	13C	33.855	0.030	6
1	H10	1H	7.405	0.161	17
1	H3	1H	8.132	0.004	16
1	H4	1H	7.613	0.005	7
1	H5	1H	7.545	0.002	8
1	H6	1H	7.949	0.003	10
1	H7	1H	7.842	0.008	11
1	H8	1H	7.444	0.007	5
1	HA	1H	4.639	0004	16
1	HB1	1H	3.667	0.003	17
1	HB2	1H	3.272	0.004	18
1	HN	1H	9.029	0.002	16
2	CA	13C	58.829	0.135	2
2	CAC	13C	166.329	0.005	2
2	CB	13C	41.620	0.133	4
2	CD	13C	52.022	0.165	4
2	CG	13C	64.939	0.015	4
2	CGC	13C	63.005	0.032	3
2	HA	1H	4.355	0.002	2
2	HB1	1H	2.744	0.003	12
2	HB2	1H	1.953	0.002	14
2	HD1	1H	3.353	0.001	12
2	HD2	1H	4.092	0.002	6
2	HN	1H	8.948	0.004	4

3	CA	13C	57.248	0.119	12
3	CAC	13C	167.534	0.162	3
3	CB	13C	39.920	0.079	4
3	CD	13C	53.836	0.046	2
3	CG	13C	62.421	0.059	3
3	CGC	13C	164.116	0.185	3
3	HA	1H	4.528	0.005	14
3	HB1	1H	2.603	0.005	10
3	HB2	1H	2.134	0.005	9
3	HD1	1H	3.479	0.004	6
3	HD2	1H	4.233	0.007	3
3	HN	1H	8.838	0.004	12
4	CA	13C	57.144	0.099	3
4	CAC	13C	168.068	0.005	3
4	CB	13C	39.911	0.084	4
4	CD	13C	53.856	0.043	2
4	CG	13C	62.325	0.002	2
4	CGC	13C	164.492	0.157	3
4	HA	1H	4.623	0.005	12
4	HB1	1H	2.567	0.004	10
4	HB2	1H	2.166	0.008	9
4	HD1	1H	3.447	0.001	5
4	HD2	1H	4.223	0.003	2
4	HN	1H	8.919	0.001	12
5	CA	13C	56.675	0.147	5
5	CAC	13C	168.078	0.042	4
5	CB	13C	36.989	0.266	6
5	CD	13C	53.789	0.038	3
5	CG	13C	60.670	0.030	5
5	CGC	13C	171.425	0.144	5
5	COE	13C	52.352	0.013	2
5	HA	1H	4.638	0.003	11
5	HB1	1H	2.493	0.005	12
5	HB2	1H	2.415	0.005	12
5	HD1	1H	3.493	0.004	8
5	HD2	1H	4.097	0.003	9
5	HE1	1H	3.583	0.002	4
5	HN	1H	8.749	0.004	15
6	CAM	13C	22.120	0.182	2
6	CNC	13C	170.053	0.034	2
6	HM1	13C	1.851	0.002	6

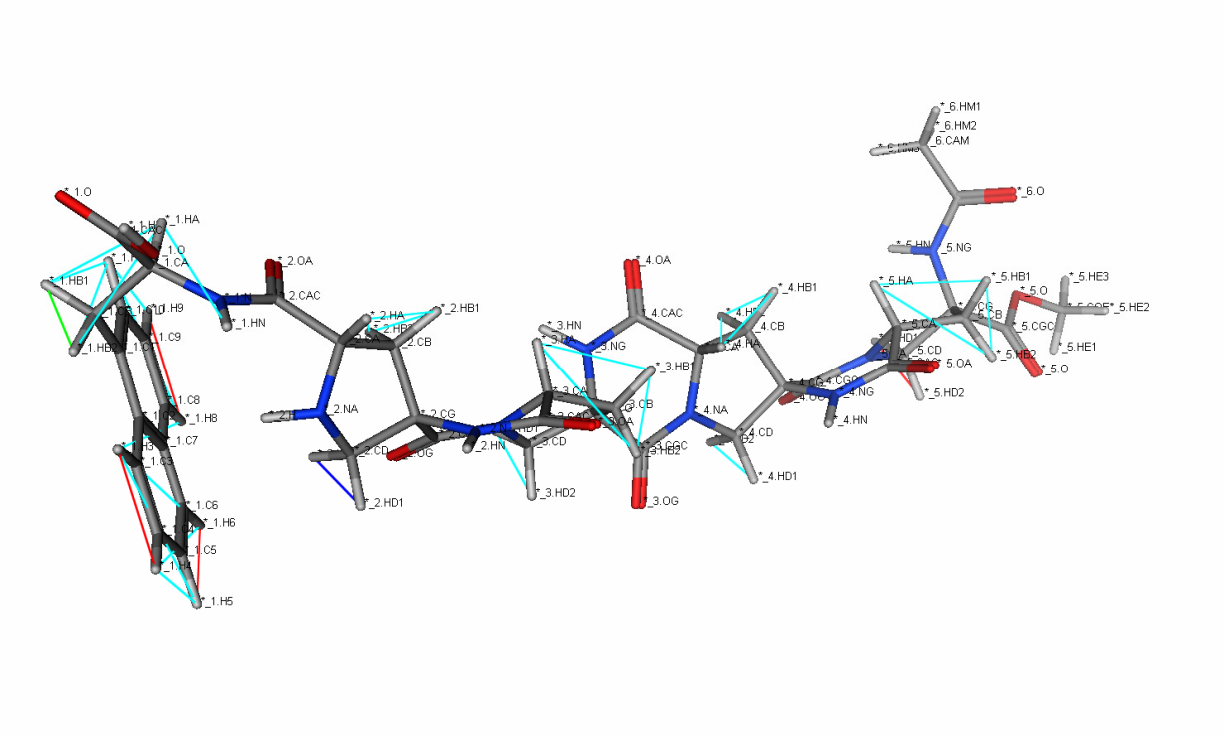

Figure 24. COSY correlations superimposed on the energy minimized structure

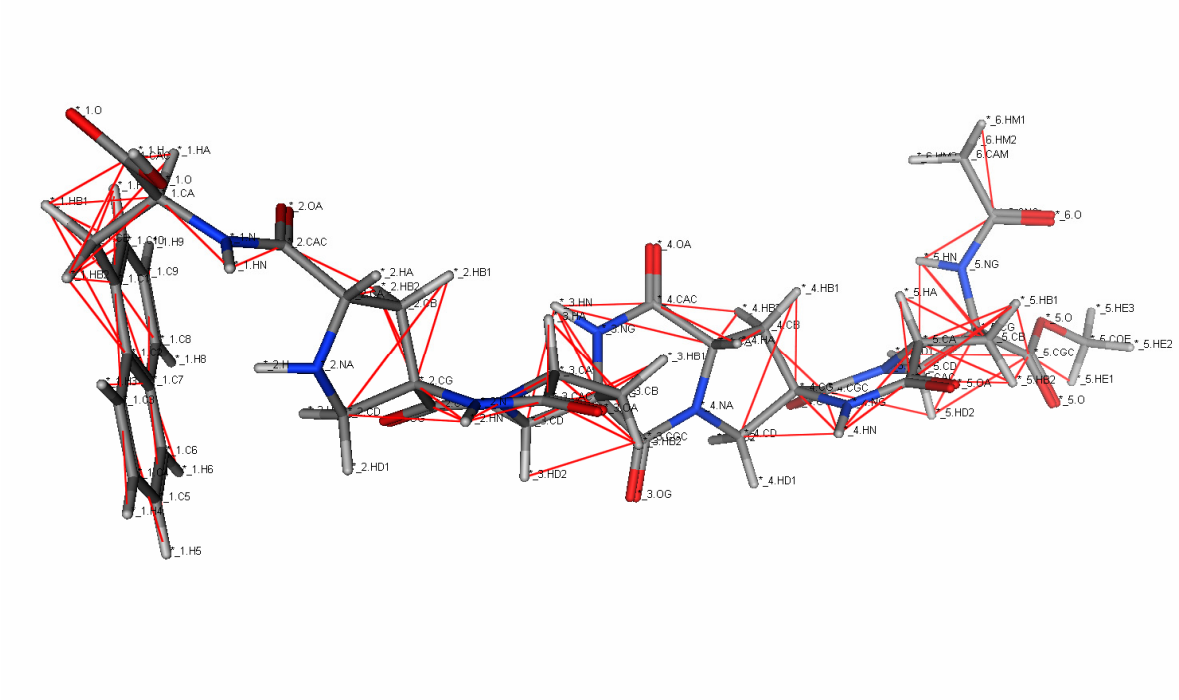

Figure 25. HMBC correlations superimposed on the energy minimized

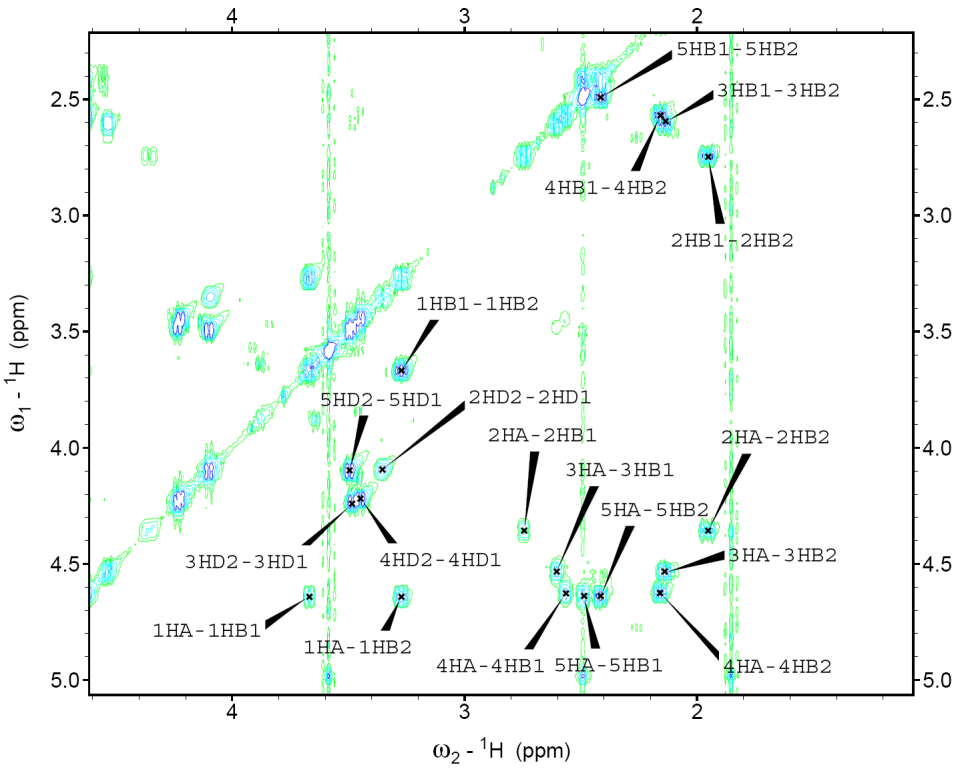

Figure 26. COSY

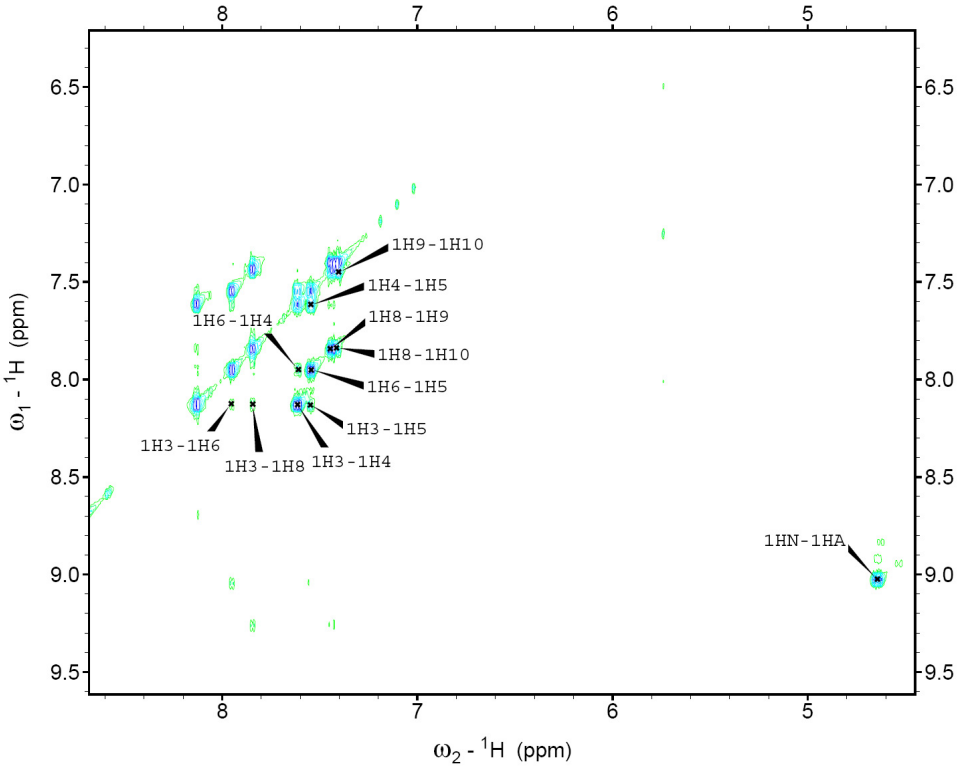

Figure 27. COSY

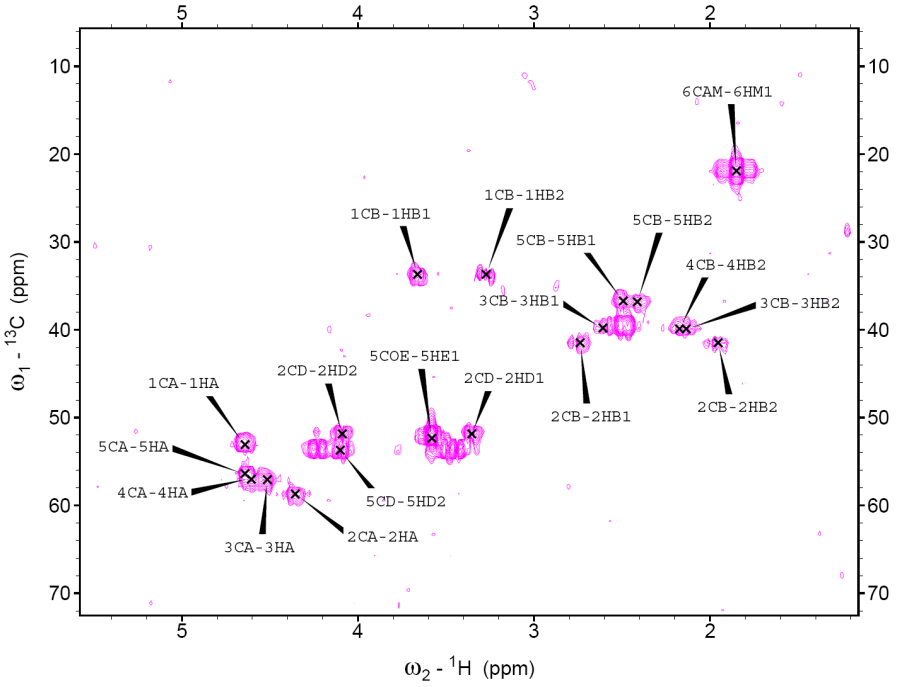

Figure 28. HMQC

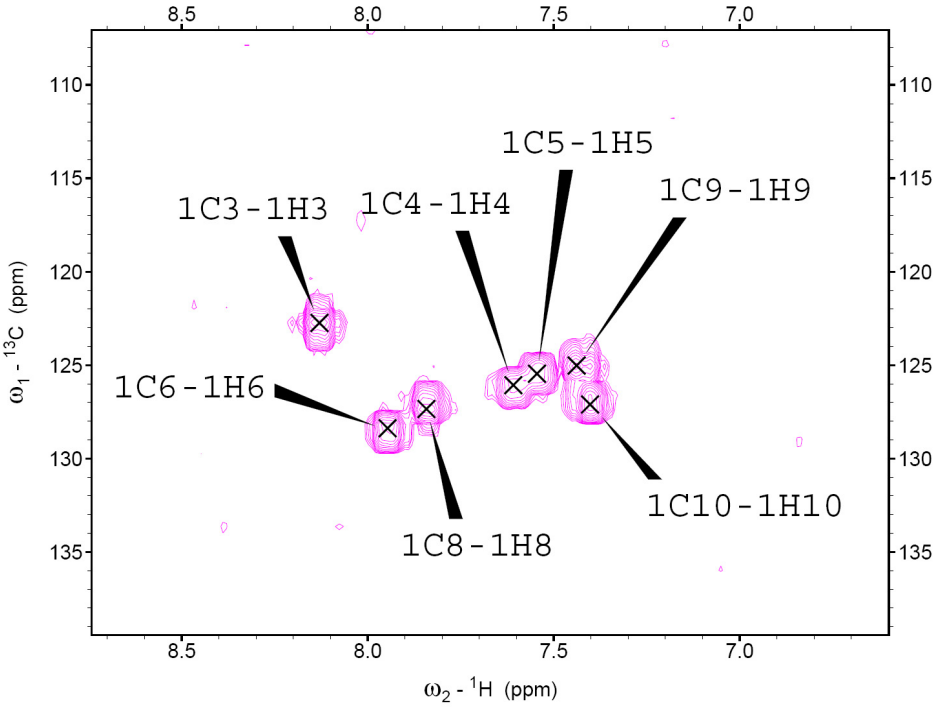

Figure 29. HMQC

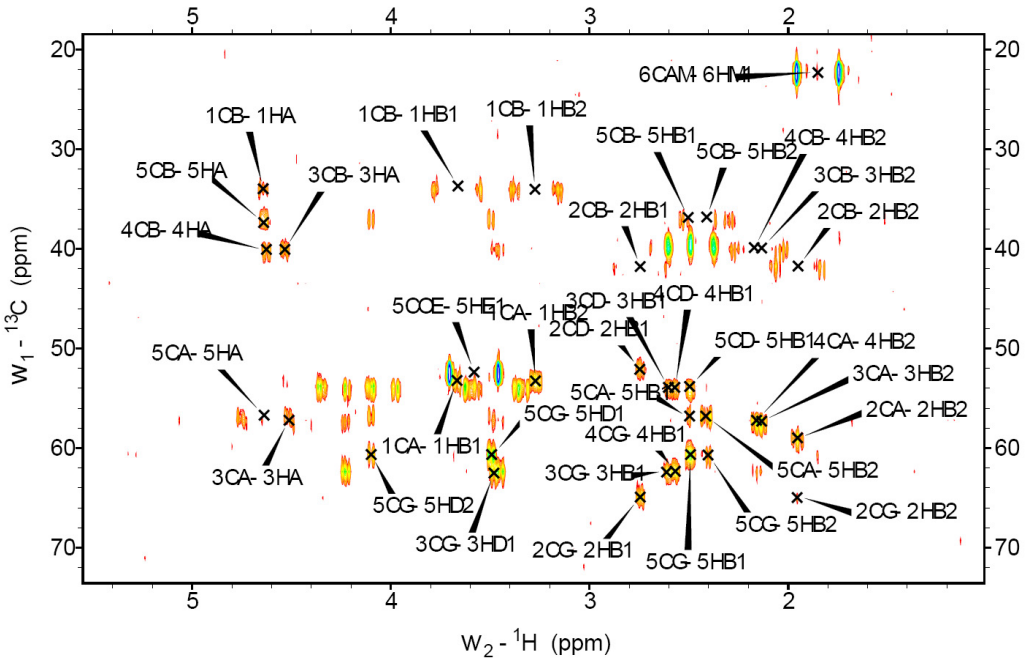

Figure 30. HMBC

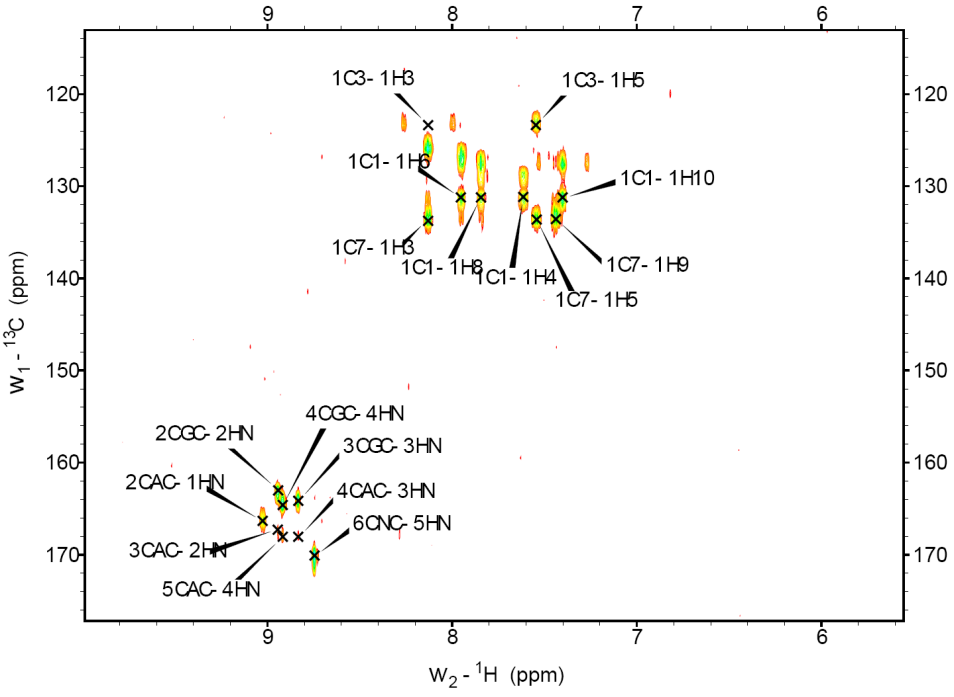

Figure 31. HMBC

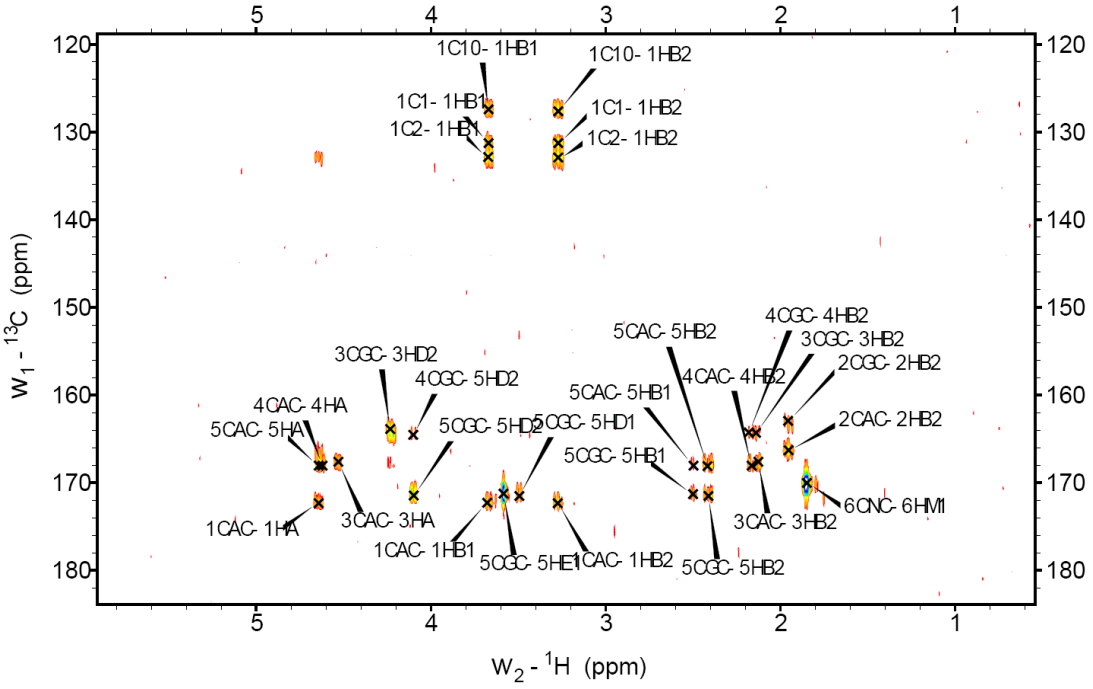

Figure 32. HMBC

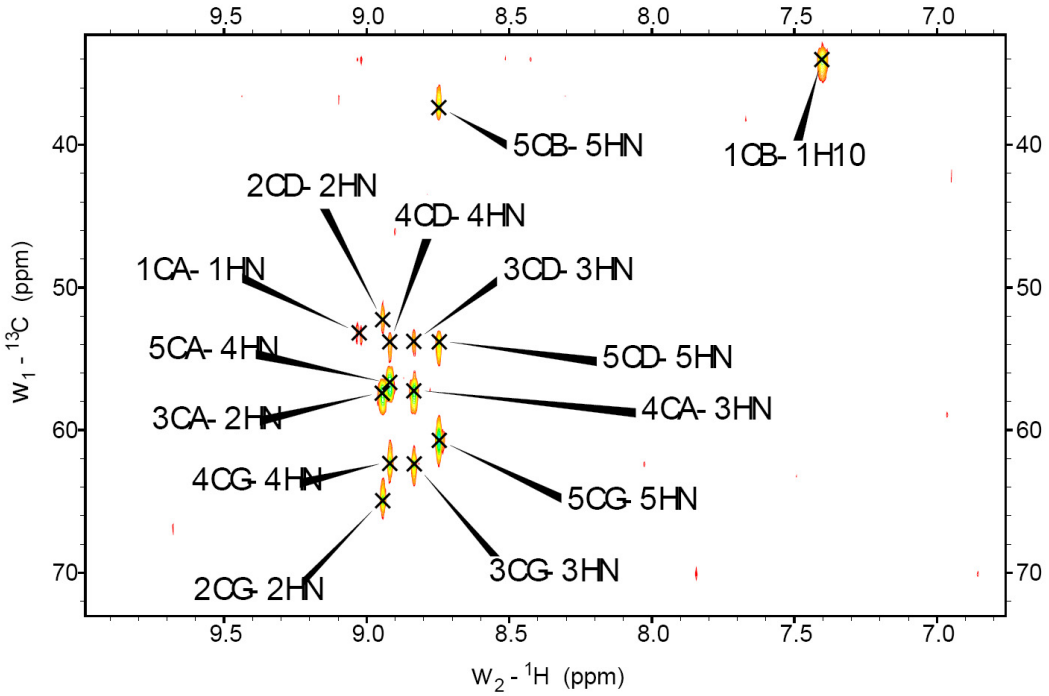

Figure 33. HMBC

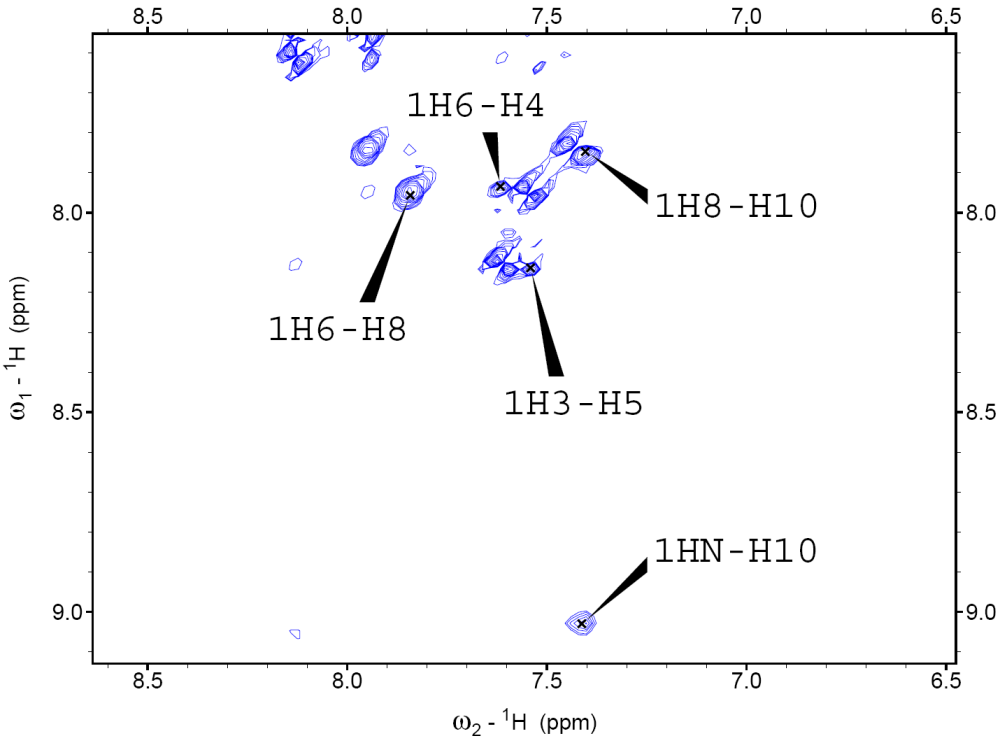

Figure 34. ROESY

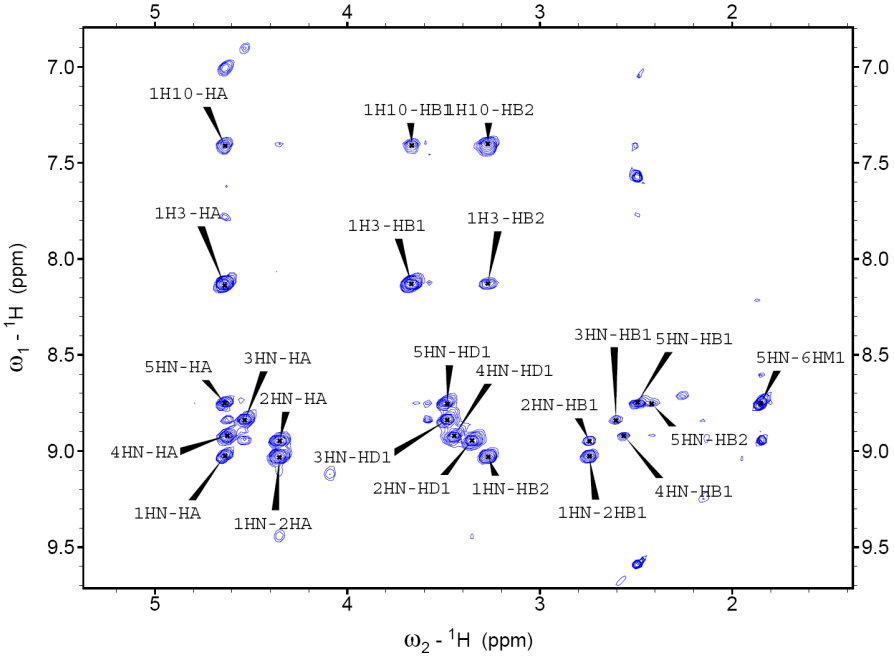

Figure 35. ROESY

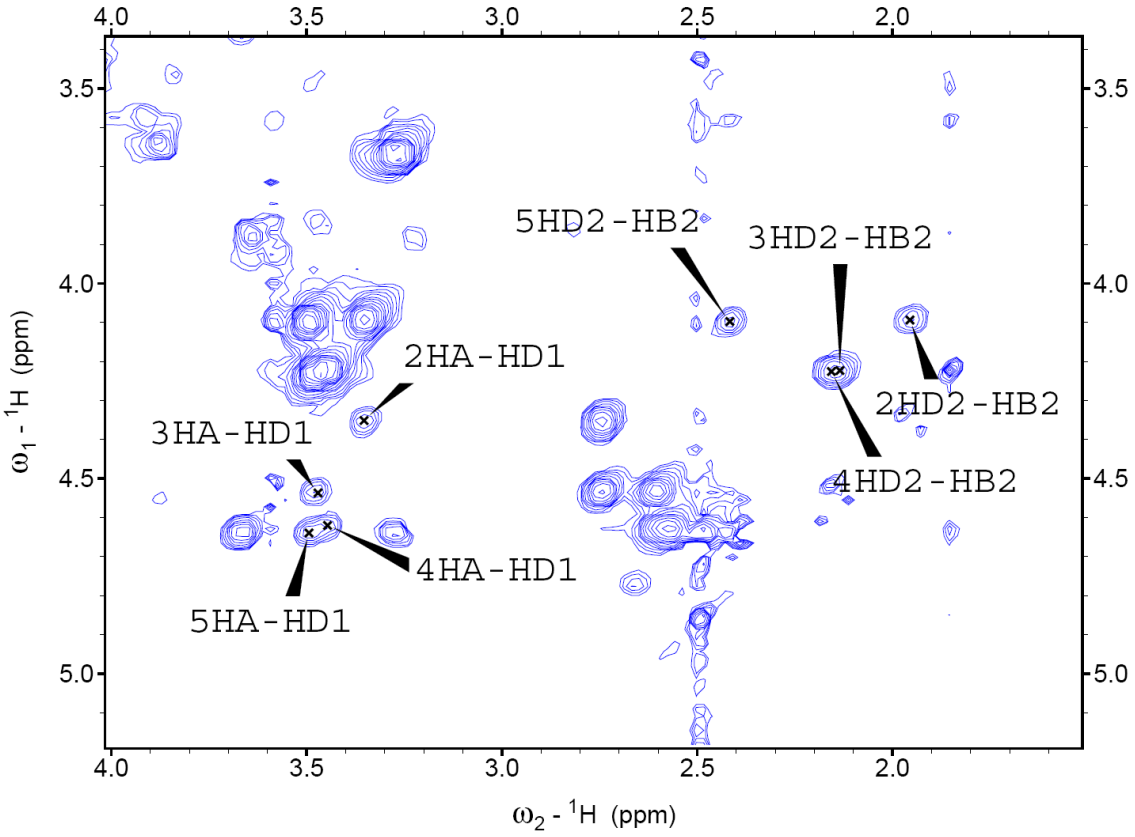

Figure 36. ROESY

BIBLIOGRAPHY

1. Voet, D.; Voet, J.; *Biochemistry*. John Wiley & Sons, Inc: New York, 1995.
2. Creighton, T. E., *Proteins: Structures and Molecular Properties*. W.H. Freeman and Company: New York, 1993.
3. van Holde, K. E.; Johnson, W. C.; Ho, P. S., *Principles of Physical Biochemistry*. Prentice Hall: Upper Saddle River, 1998.
4. Balzani, V.; Credi, A.; Venturi, M., Wiley-VCH: Weinheim, 2003.
5. Gellman, S. H., . *Acc. Chem. Res.* **1998,** 31, 173-180.
6. Appella, D. H.; Christianson, L. A.; Klein, D. A.; Powell, D. R.; Huang, X.; Barchi, J. J.; Gellman, S. H., *Nature* **1997,** 387, 381-384.
7. Appella, D. H.; Barchi, J. J.; Durell, S. R.; Gellman, S. H., *J. Am. Chem. Soc.* **1999,** 121, 2309-2310.
8. Gude, M.; Piarulli, U.; Potenza, D.; Salom, B.; Gennari, C., *Tet. Lett.* **1996,** 36, 8589-8592.
9. Smith, A. B. I.; Guzman, M. C.; Sprengeler, P. A.; Keenan, T. P.; Holcomb, R. C.; Wood, J. L.; Carroll, P. J.; Hirschmann, R., *J. Am. Chem. Soc.* **1994,** 116, 9947-9962.
10. Hamuro, Y.; Geib, S. J.; Hamilton, A. D., *J. Am. Chem. Soc.* **1996,** 118, 7529-7541.
11. Nowick, J. S.; Holmes, D. L.; Mackin, G.; Noronha, G.; Shaka, A. J.; Smith, E. M., *J. Am. Chem. Soc.* **1996,** 118, 2764-2765.
12. Nowick, J. S.; Abdi, M.; Bellamo, K. A.; Love, J. A.; Martinez, E. J.; Noronha, G.; Smith, E. M.; Ziller, J. W., *J. Am. Chem. Soc.* **1995,** 117, 89-99.
13. Nowick, J. S.; Smith, E. M.; Noronha, G., *J. Org. Chem.* **1995,** 60, 7386-7387.
14. Nowick, J. S.; Mahrus, S.; Smith, E. M.; Ziller, J. W., *J. Am. Chem. Soc.* **1996,** 118, 1066-1072.
15. Nowick, J. S.; Powell, N. A.; Martinez, P. E.; Smith, E. M.; Noronha, G., *J. Org. Chem.* **1992,** 57, 3763-3765.
16. Prince, R. B.; Okada, T.; Moore, J. S., *Angew. Chem. Int. Ed.* **1999,** 38, 233-236.
17. Nelson, J. C.; Saven, J. G.; Moore, J. S.; Wolynes, P. G., *Science* **1997,** 277, 1793-1796.
18. Hagihara, M.; Anthony, N. J.; Stout, T. J.; Clardy, J.; Schreiber, S. L., *J. Am. Chem. Soc.* **1992,** 114, 6568-6570.
19. Nowick, J.S.; V. A., Noronha, G.; Ziller, J.W. *J. Org. Chem.* **1995,** 60, 1888-1890.
20. Nowick,J.S.; Smith, E.M; Noronha, G. *J. Org. Chem.* **1995,** 60, 7386-7387.
21. Fan, E.; Van Arman, S. A.; Kincaid, S.; Hamilton, A. D., *J. Am. Chem. Soc.* **1993**, (115), 369-370.
22. Adrian, J. C.; Wilcox, C. S., *J. Am. Chem. Soc.* **1989,** 111, 8055-8057.
23. Levins, C.G.; Schafmeister, C. E. *J. Am. Chem.Soc.* **2002,** 125, 4702-4703.

24. Levins,C.G.; Schafmeister, C. E. *J. Org. Chem.* **2005,** 70, 9002-9008.
25. Levins, C.G.; Brown, Z. Z; Schafmeister, C.E. *Org. Lett.* **2006,** 8, (13), 2807-2810.
26. Gupta, S.; Das, B.C.; Schafmeister, C.E. *Org. Lett.* **2005,** 7, (14), 2861-2864.
27. Habay, S.A.; Shafmeister, C.E. *Org. Lett.* **2004,** 6, (19), 3369-3371.
28. Paquet, A., *Can. J. Chem* **1982**, 976-980.
29. Merrifield, R. B., *J. Am. Chem. Soc.* **1963,** 85, 2149-2154.
30. Fischer, P. M., *J. Pept. Sci.* **2003,** 9, 9-35.
31. Dinsmore, C. J.; Beshore, D. C., *Tetrahedron* **2002,** 58, 3297-3312.
32. Gund, P.; Veber, D. F., *J. Am. Chem. Soc.* **1979,** 101, 1885-1887.
33. Gupta, S.; Macala, M.; Schafmeister, C. E., *J. Org. Chem.* **2006,** 71, 8691-8695.
34. Schafmeister, C. E. *CANDO*, University of Pittsburgh: Pittsburgh, 2005.
35. Chemical Computing Group. *MOE*, 6; Montreal, 2005.
36. Wagner, G.; Pardi, A.; Wuthrich, K., *J. Am. Chem. Soc.* **1983,** 105, 5948-5949.
37. Moriuchi, T.; Tamura, T.; Hirao, T., *J. Am. Chem. Soc.* **2002,** 124, 9356-9357.